Frontiers of Physics
https://doi.org/10.1007/s11467-019-0901-8
Front. Phys.
14(5), 53401 (2019)

REVIEW ARTICLE

Recent advances in controlling the crystallization of two-dimensional perovskites for optoelectronic device

Shi-Qiang Luo[1,*], **Ji-Fei Wang**[1,2,*], **Bin Yang**[3,4], **Yong-Bo Yuan**[1,†]

[1] *Hunan Key Laboratory of Super Microstructure and Ultrafast Process, School of Physics and Electronics, Central South University, Changsha* 410083, *China*
[2] *College of Physic and Electric Information, Hunan Institute of Science and Techenology, Yueyang* 414006, *China*
[3] *College of Materials Science and Engineering, Hunan University, Changsha* 410082, *China*
[4] *Hunan Province Key Laboratory for Advanced Carbon Materials and Applied Technology, Hunan University, Changsha* 410082, *China*
Corresponding author. E-mail: [†] *yuanyb@csu.edu.cn*
Received March 15, 2019; accepted April 18, 2019

Though three-dimensional (3D) organic–inorganic halide perovskites (OIHP) is very promising for low cost and distributed PV generation, the stability issue of 3D OIHP is still a problem for its commercialization. Two-dimensional (2D) perovskites, protected by periodic organic ligands, is promising due to its excellent optoelectronic property and superior stability. However, 2D perovskite is anisotropic in its crystal structure and optoelectronic properties, and the resulted film is often a mixture of different phase. So, methods to manipulate 2D perovskite crystal orientation and its phase separation are vital. In this review, the major advances on the composition engineering, crystal orientation, phase separation, and interfacial capping are summarized. Besides, efforts on understanding the formation process of 2D perovskite crystal are also discussed, which is important for making full use of 2D perovskite in functional optoelectronic devices.

Keywords optoelectronic devices, perovskite solar cells, nanoscale materials, chemical vapor deposition

Contents

1 Introduction

Perovskite is a general term for a class of crystal structures with formula of ABX_3, which was named in 1830s by Gustav Rose in honor of Russian mineralogist, L. A. Perovski [1]. Those perovskite crystals have a similar crystal structure as that of calcium titanate ($CaTiO_3$). The first inorganic halide perovskite cesium lead halide ($CsPbX_3$) (X = Cl^-, Br^- or I^-) and the first organic-inorganic hybrid perovskite (OIHP) methylammonium lead halide ($MAPbX_3$) (MA = $CH_3NH_3^+$; X = Cl^-, Br^- or I^-) were reported in 1958 and 1978, by Moller [2] and Weber [3], respectively. In 1990s, Mitzi and coworkers extended the OIHP family with 2D perovskite structure and applied the 2D perovskite to thin film transistor and light-emitting diodes (LEDs) [4–6]. However, OIHP did not receive broad attention until 2009 when the first OIHP sensitized solar cells were reported by Miyasaka *et al.* [7] with $MAPbBr_3$ and $MAPbI_3$ as the "dyes". The ABX_3 structure of perovskite was composed by corner shared $[BX_6]^{4-}$ octahedrons along with A^+ cation filling the voids, as shown in Fig. 1(a) [8]. The structure stability of ABX_3 can be evaluated by Goldschmidt's tolerance factor $t = (r_A + r_X)/[\sqrt{2}(r_B + r_X)]$ and the octahedral factor $\mu = r_B/r_X$, where r_A, r_B, and r_X are the ionic radii of the corresponding ions [9], respectively. To achieve 3D perovskite structure of ABX_3, t and μ should empirically satisfy $0.80 \leq t \leq 1.0$ and $0.44 \leq \mu \leq 0.90$, respectively. Thus, when the radii of A cation excessed a critical size, low-dimensional perovskite structures (0D, 1D and 2D)

*These authors contributed equally to this work. Special Topic: Solar Energy Storage and Applications (Eds. Min Liu and Haotian Wang).

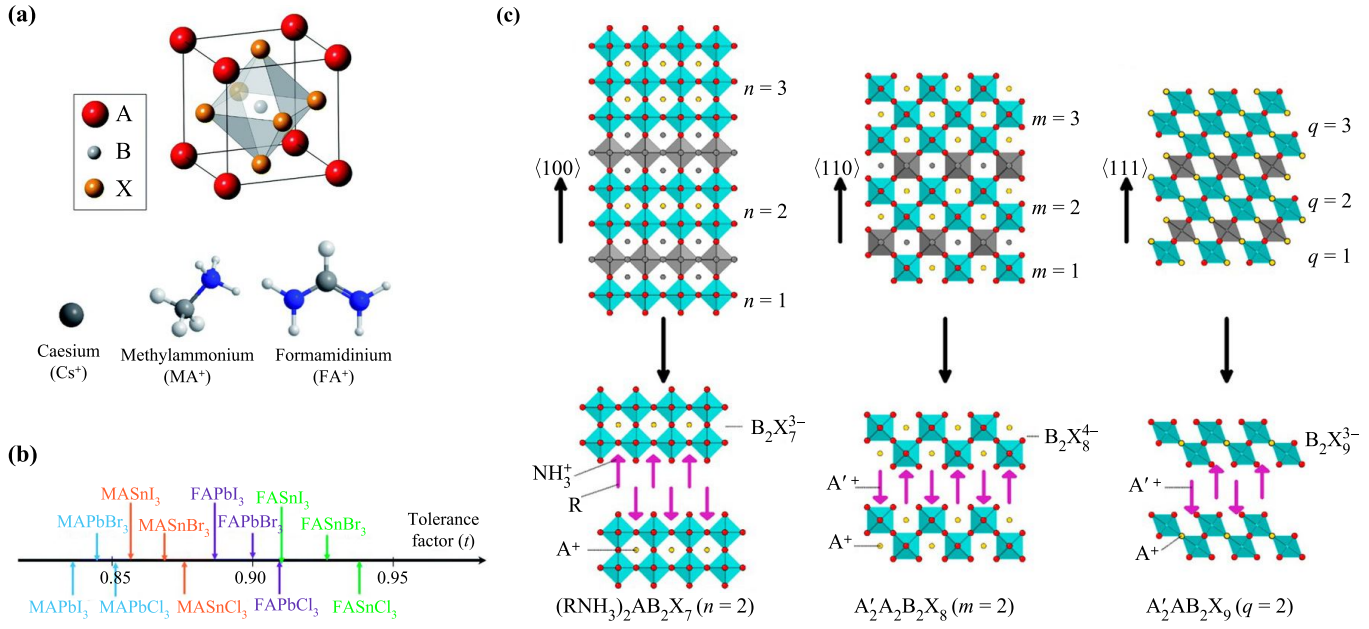

Fig. 1 **(a)** The crystal structure of 3D perovskite ABX_3, with A cation of caesium (Cs^+), methylammonium (MA^+), or formamidinium (FA^+). Reproduced with permission from Ref. [8], Copyright © 2014 The Royal Society of Chemistry. **(b)** Tolerance factors (t) of a series of 3D halide perovskites. Reproduced with permission from Ref. [9], Copyright © 2015 The Royal Society of Chemistry. **(c)** The structure derivation of layered 2D perovskite with long cation cutting the 3D perovskite from (100), (110) and (111) plane, respectively. Reproduced with permission from Ref. [12], Copyright © 2016 American Chemical Society.

would form [10, 11]. The 2D perovskites can be categorized by the cutting plane of 3D structure as shown in Fig. 1(c) [12, 13]. For 2D OIHP, the Dion–Jacobson (DJ) phases were distinguished from the Ruddlesden–Popper (RP) phases [14], where DJ phases possess divalent long-chain cation and inorganic perovskite slabs show little displacement between each other. This review will mainly focus on the controlled formation of (100)-oriented 2D OIHP, which can be expressed as $A'_2A_{n-1}B_nX_{3n+1}$ or $A''A_{n-1}B_nX_{3n+1}$, where A′ and A″ are 1+ and 2+ valent aromatic or aliphatic alkyl ammonium cations, respectively. The ammonium cations slice the 3D perovskite phase ABX_3 into quantum wells (QWs) with inorganic BX_6 octahedrons layer number of n.

The rapid development of perovskite solar cells promoted the research of perovskite optoelectronic devices such as LEDs [15–17], photodetectors [18–24], field effect transistors [25–27] and other photonic devices [28]. However, the instability of 3D perovskite impeded its commercialization [29–32]. To improve the intrinsic stability of hybrid perovskites, RP perovskite combined both high performance and stability gradually becomes the frontier of current research. First principles calculation showed that the formation energy of RP perovskite decreased with increasing of layer number n [33], which predicted that better thermal dynamic stability of RP perovskite than 3D perovskite. Bulky hydrophobic ammonium cations can cause steric effects and strain the Pb-I bonds at the surface, which effectively hinders the diffusion of water molecules [34]. The improved stability against moisture in 2D perovskites than that of $MAPbI_3$ has been demonstrated in the cases of $PEA_2MA_{n-1}Pb_nI_{3n+1}$ (PEA^+: phenylethylammonium) [35] and $BA_2MA_{n-1}Pb_nI_{3n+1}$ (BA^+: n-butylammmonium) [36]. Moreover, the tunable bandgap and the higher exciton binding energy of 2D perovskite enabled its application to LEDs [37, 38]. However, the power conversion efficiency of solar cells based on 2D perovskite still lagged behind that of 3D perovskite solar cells, resulting from inferior charge transport efficiency. Since the insulating organic spacing layers sandwiched between BX_6 octahedrons layers cause significant anisotropic charge transporting in RP perovskites, vertically or horizontally orientated QWs of RP perovskite were particularly suitable for optoelectronic device with different configurations and functions. Therefore, the orientations of 2D perovskite crystal need to be well controlled to satisfy the different charge transport demands. This review aimed to summarize the recent advances in controlling the crystallization of 2D perovskite.

2 Tunable composition and bandgap of 2D perovskites

For 2D perovskite with formula of $A'_2A_{n-1}B_nX_{3n+1}$ or $A''A_{n-1}B_nX_{3n+1}$, considerable researches have been devoted to the exploring of new 2D materials intermediated by different A′ cations. The employed long-chain

cations A′ were well summarized in Ref. [13]. Replacing the cations on A′ or A″ site does not contribute directly to the electronic structures of 2D perovskites. According to first principle calculation, the conduction band minimum of $MAPbI_3$ is mainly composed of nonbonding 6p-orbitals of lead (Pb) and the valence band maximum mainly comes from the anti-bonding of the hybridized Pb 6s and iodine (I) 5p orbitals. The MA^+ cation just functioned as charge compensator and influenced the band gap indirectly by size effect, i.e., A^+ cation usually affect the metal-halide-metal bond angle with its volume [39, 40]. Although the long chain cations also don't contribute directly to the formation of perovskite band structures, they can subtly influence the electronic structure of perovskites and hence their photoluminescence (PL) peak position by: (i) distorting the inorganic lattice and change the electron cloud overlapping between Pb-I bonds [41]; (ii) the strong quantum and dielectric confinement caused by the intrinsic 2D crystal structures of RP perovskites or the morphological dimensions, which cause the band gap to increase. Taking BA^+ as long-chain cation as example, the band gap increased from 1.59 eV for $MAPbI_3$ to 1.85 eV for $BA_2MA_3Pb_4I_{13}$ ($n = 4$) and then to 2.35 eV for BA_2PbI_4 ($n = 1$) [37]. The exciton binding energy (E_B) can be obtained by the difference in energy of the absorption edge to the emission maximum as shown in Figs. 2(a) and (b). It was found that the E_B of 2D perovskite increases from 10 meV to 80 meV with decreasing n from 4 to 1 [37]. Besides layer number n, both metal and halide ions can also modify the band gap of RP perovskites, as shown in Figs. 2(c) and (d) [42]. Similar with $BA_2MA_{n-1}Pb_nI_{3n+1}$, the band gap modification by layer number was also reported for $POEA_2MA_{n-1}Pb_nBr_{3n+1}$ ($POEA^+$: 2-phenoxyethylamine) [43] and 2D $MAPbBr_3$ nanoplates [44]. Controlling the average layer number ($\langle n \rangle$) of 2D perovskite is usually achieved by adding different amount of long-chain cations in precursor solution [37, 43, 45] or in anti-solution [44]. For the long-chain cation, the high dipole moment 2, 2, 2-trifluoroethylamine cations might attract charges, in which way, the exciton binding energy of RP perovskite could be reduced [46]. Moreover, when the distance between neighboring inorganic layers was shorten by applying small propane-1, 3-diammonium cations, a weaker quantum confinement was

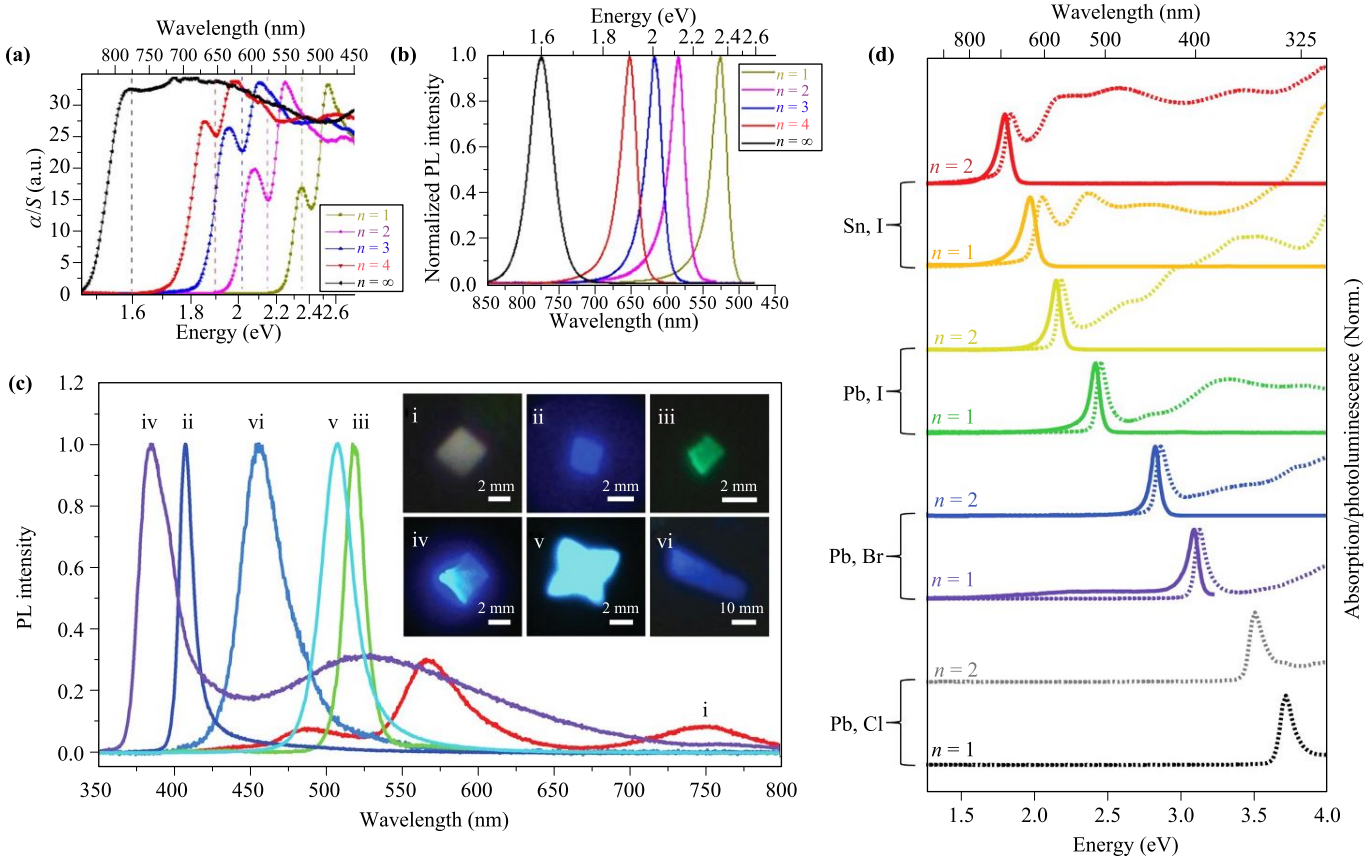

Fig. 2 **(a, b)** The absorption and photoluminescence spectra of $BA_2MA_{n-1}Pb_nI_{3n+1}$ (n = 1–4, 3D). Reproduced with permission from Ref. [37], Copyright © 2016 American Chemical Society. **(c)** Solution phase PL spectra and optical PL images (insets) of 2D perovskite nanoplates of BA_2PbCl_4 (i), BA_2PbBr_4 (ii), BA_2PbI_4 (iii), $BA_2PbCl_2Br_2$ (iv), $BA_2PbBr_2I_2$ (v), and $BA_2MAPb_2Br_7$ (vi). Reproduced with permission from Ref. [42], Copyright © 2015 American Association for the Advancement of Science. **(d)** Solution phase absorption and photoluminescence spectra of $L_2[ABX_3]_{n-1}BX_4$, where L is an organic ligand (octylammonium, butylammonium). Reproduced with permission from Ref. [45], Copyright © 2016 American Chemical Society.

proposed, which might enable the efficient charge transport between neighboring inorganic layers [47].

3 Controlled thin-film orientation

3.1 Out-of-plane orientation

Out-of-plane (OP) orientation is defined as the vertical alignment of QWs, which are composed by inorganic BX_6 octahedrons layer, with respect to the plane of the substrates [as shown in Fig. 3(a)] [48]. Since the charge transport is limited within the QWs, the OP orientation of QWs of RP perovskites is quite desirable for high efficient vertical-structure-based optoelectronic devices, such as perovskite solar cells. For the first demonstration of RP perovskite solar cells (PSCs), the power conversion efficiency (PCE) was modest 4.73% [35]. Later, RP PSCs based on $BA_2MA_{n-1}Pb_nI_{3n+1}$ with a similar PCE of 4.02% was reported [36]. In those studies, mixed solvent of nitromethane/acetone [35] or a high concentration of precursor solution (1.8 M Pb^{2+}) [36] was adopted, X-ray diffraction (XRD) patterns demonstrate the presence of RP perovskite with OP orientation since clear (111) and (202) diffraction peaks were observed. Probably, the inferior short circuit current (Jsc) and fill factor (FF), which limited the PCEs of the early RP PSCs, is attributed to the non-ideal orientation regions or misalignment of QWs, as shown in Figs. 3(c) and (d) [49, 50].

In 2016, a dramatically improved PCE of 12.5% for RP perovskite solar cells based on $BA_2MA_{n-1}Pb_nI_{3n+1}$ ($n = 4$) was achieved by hot-casting method [48]. Preferential OP orientation of RP perovskite was supported by grazing-incidence wide-angle X-ray scattering (GIWAXS) [as shown in Fig. 3(b)] for the first time [48]. This hot casting method then initiated a lot of related investigations with a purpose of further improving the solar cell performance. By partially replacing MA^+ with FA^+ (formamidinium) [51] or Cs^+ (cesium) [52], the PCEs of $BA_2MA_3Pb_4I_{13}$ perovskite solar cells were further improved to 12.8% and 13.7%, respectively. All the achievements suggested that the RP perovskite can adopt an OP orientation and offer a promising charge transport and hence a high PCE. After this encouraging discovery, an increasing number of methods beyond hot-casting method have been developed. It should be emphasized that applying additives such as such as HI [53, 54], NH_4SCN [55–57], MACl [58, 59], or solvent engineering [49, 60, 61] has been found to also enable OP orientation. Apart from the different methods to achieve OP orientation of RP perovskite, some common results were shared by different reports. When the high concentration of precursor solution was spin-coated at room temperature (RT), in-plane (IP) orientation was observed for $BA_2MA_{n-1}Pb_nI_{3n+1}$ ($n = 1, 2$) and OP orientation was showed for $BA_2MA_{n-1}Pb_nI_{3n+1}$ ($n = 3, 4$) perovskite

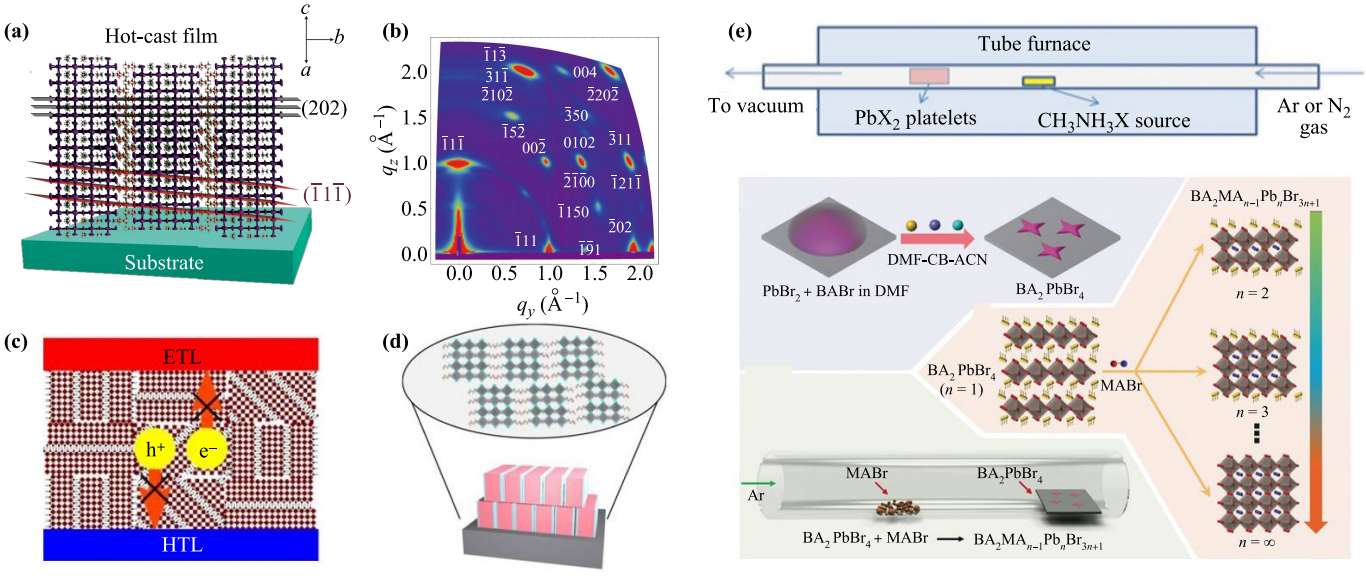

Fig. 3 **(a, b)** Scheme of orientation and grazing-incidence wide-angle X-ray scattering (GIWAXS) patterns for $BA_2MA_3Pb_4I_{13}$ perovskite film by hot-casting method. Reproduced with permission from Ref. [48], Copyright © 2016 Springer Nature. **(c)** Scheme of disordered orientation of $BA_2MA_3Pb_4I_{13}$ perovskite film prepared by room-temperature casting method. Reproduced with permission from Ref. [49], Copyright © 2018 Springer Nature. **(d)** Scheme of vertically packed quantum wells with misalignment in molecular structures. Reproduced with permission from Ref. [50], Copyright © 2018 Springer Nature. **(e)** Schematic of the synthesis setup for converting PbX_2 platelets by MAX vapor. Reproduced with permission from Ref. [73], Copyright © 2014 John Wiley and Sons. **(f)** Scheme of synthesis of BA_2PbBr_4 perovskites via a ternary solvent method and transformation of BA_2PbBr_4 into $BA_2MA_{n-1}Pb_nBr_{3n+1}$ perovskites via chemical vapor deposition of MABr. Reproduced with permission from Ref. [78], Copyright © 2017 John Wiley and Sons.

film [36]. IP orientation preference for low layer number ($n = 1, 2$) was also observed for hot-casting method [52]. The orientation preference was inferred to the competition between the BA ions, which try to confine the growth within the planar layer, and the MA ions, which try to expand the perovskite QWs growth outside the layer [36]. For RT spin-coated $ThMA_2MA_2Pb_3I_{10}$ ($ThMA^+$: 2-thiophenemethylammonium), a dense web of nanorod-like film was formed when 0.33 molar ratio of $MACl/Pb^{2+}$ was added [59]. The nanorod-like crystals were also observed for $BA_{0.05}(FA_{0.83}Cs_{0.17})_{0.95}Pb(I_{0.8}Br_{0.2})_3$ film with HI as additive [62]. The nanorod-like crystals were regarded as OP oriented RP perovskite [59, 62]. For hot-casting method, appropriate amount of dimethyl sulfoxide (DMSO) in perovskite precursor solution promote OP orientation of $BA_2MA_{n-1}Pb_nI_{3n+1}$ perovskite [52, 63, 64]. When 6.7 vol% of DMSO was added into dimethylformamide (DMF) as solvent, and meanwhile 0.1 molar ratio of $MACl/Pb^{2+}$ was added, OP orientation of $PEA_2MA_3Pb_4I_{13}$ was achieved by RT spin-coating method [58]. When dimethylacetamide (DMAc) was applied as solvent, the nucleation and crystal growth was found to arising from the liquid–air interface [49]. The top-down crystal growth process was also observed when $BA_2MA_3Pb_4I_{13}$ perovskite DMF precursor solution was deposited on PEDOT substrate at 50 °C [65]. On the other hand, for hot-casting method, a bottom to top crystallization process initiated by bonding of $BA_2MA_3Pb_4I_{13}$ perovskite with TiO_2 was also proposed as an alternative explanation [64]. When both MACl as additive and hot-casting method was applied for $(3BBA)_2MA_{n-1}Pb_nI_{3n+1}$ ($n \approx 3$, $3BBA^+$: 3-bromobenzylammonium) film, perovskite grains grown perpendicular to the substrate at the bottom region of the film was observed from cross-sectional scanning transmission electron microscope (STEM) [66]. For NH_4SCN additive, OP orientation was achieved for both $PEA_2MA_{n-1}Pb_nI_{3n+1}$ ($n = 3, 4, 5$) [55] and $BA_2MA_{n-1}Pb_nI_{3n+1}$ ($n = 3, 4$) [57]. Moreover, NH_4SCN can more effectively drive the $PEA_2MA_4Pb_5I_{16}$ thin film into a vertically orientated 2D structure [56]. Detailed information about PSCs based on OP oriented small-$\langle n \rangle$ RP perovskite mentioned above was summarized in Table 1.

Though many strategies for facilitating the OP orientation of RP perovskite have been reported, the in-depth understanding of the mechanism about OP orientation is still sparse. For the IP orientation of $BA_2MA_{n-1}Pb_nI_{3n+1}$ ($n = 1, 2$) [36], the competition mechanism between the BA^+ and MA^+ ions on orientation was left less explained. For the nucleation and crystal growth initiated from the liquid–air interface [49], it was observed that a low supersaturation of perovskite precursor solution beneath the nucleation at the liquid-air interface was necessary to crystallize vertically oriented thin films [67], however the driving force for the OP orientation is still unknown. For the proposed bottom to top crystallization process [64], the proposed mechanism cannot be used to explain the OP orientation of RP perovskite

Table 1 Summary of RP perovskite solar cells base on RP perovskites with $\langle n \rangle = 3$–5.

Solar cell structure*	Method#	V_{oc} (V)	J_{sc} (mA/cm^2)	FF (%)	PCE (%)	Ref.
FTO/c-TiO_2/$PEA_2MA_2Pb_3I_{10}$/spiro/Au	RC	1.18	6.72	60	4.73	[35]
FTO/c-TiO_2/m-TiO_2/$BA_2MA_2Pb_3I_{10}$/spiro/Au	RC	0.929	9.42	46	4.02	[36]
FTO/PEDOT:PSS/$BA_2MA_3Pb_4I_{13}$/PCBM/Al	HC	1.01	16.76	74.13	12.51	[48]
ITO/PEDOT:PSS/$BA_2MA_3Pb_4I_{13}$ w 20% FA^+/PCBM/BCP/Ag	Hot-casting	0.999	18.12	70.79	12.81	[51]
FTO/c-TiO_2/$BA_2MA_3Pb_4I_{13}$ w 5% Cs^+/spiro/Au	Hot-casting & DMSO	1.08	19.95	63.47	13.68	[52]
FTO/C_{60}/$(iso\text{-}BA)_2MA_3Pb_4I_{13}$/spiro/Au	HC & HI	1.2	16.54	53.54	10.63	[54]
ITO/PEDOT:PSS/$PEA_2MA_4Pb_5I_{16}$/PCBM/BCP/Ag	RC & NH_4SCN	1.11	15.01	67	11.01	[55]
ITO/PEDOT:PSS/$PEA_2MA_4Pb_5I_{16}$/PCBM/BCP/Ag	RC & NH_4SCN+NH_4Cl	1.19	15.8	75	14.7	[56]
ITO/PEDOT:PSS/$BA_2MA_3Pb_4I_{13}$/PCBM/BCP/Ag	RC & NH_4SCN	0.98	14.71	61	8.79	[57]
ITO/PEDOT:PSS/$PEA_2MA_3Pb_4I_{13}$/PCBM/BCP/Ag	RC & DMSO & MACl	1.16	14.7	71	12.1	[58]
ITO/PEDOT:PSS/$ThMA_2MA_2Pb_3I_{10}$/PCBM/BCP/Ag	Anti-solvent & MACl	1.07	18.89	76.3	15.42	[59]
ITO/NiO_x/$BA_2MA_3Pb_4I_{13}$/PCBM:ICBA/BCP/Ag	HC & DMAc NMP	1.23	13.61	72.17	12.07	[60]
ITO/PTAA/$(3BBA)_2MA_2Pb_3I_{10}$/PCBM/Cr/Au	HC & MACl	1.23	18.22	81.2	18.20	[66]
ITO/PEDOT:PSS/$BA_2MA_3Pb_4I_{13}$/PCBM/PEIE/Ag	RT SC & hot substrate	1.14	18.8	69.5	14.9	[65]
ITO/PEDOT:PSS/$BA_2MA_4Pb_5I_{16}$/PCBM/Al	HC & DMSO	0.986	15.5	65.5	10.0	[63]
ITO/PEDOT:PSS/(PDA)$MA_2Pb_3I_{10}$/C_{60}/BCP/Ag	RC & MACl	0.97	18.0	74.3	13.0	[47]

*c-: compact, m-: mesoporous, spiro: 2, 2, 7, 7′-Tetrakis(N,N-di-p-methoxyphenylamine) 9, 9′-spirobifluorene, PEDOT-PSS: poly(3, 4-ethylenedioxythiophene)-poly(styrenesulfonate) $ThMA^+$: 2-thiophenemethylammonium ICBA: (indene-C60 bisadduct), PTAA: poly [bis(4-phenyl)(2, 4, 6-trimethylphenyl)amine], PEIE: polyethylenimine ethoxylated, PDA: propane-1,3-diammonium, 3BBA: 3-bromobenzylammonium.

#RC: room temperature spin-coating, HC: hot-casting, NMP: N-methyl pyrrolidine.

on poly(3, 4-ethylenedioxythiophene) (PEDOT) substrate [48] or nickel oxide (NiO_x) substrate [60], where the bonding of $BA_2MA_3Pb_4I_{13}$ perovskite with TiO_2 was absent. Therefore, the most favoured grow direction of RP perovskite (top-down or bottom-up) is also confusing. The difficulty for understanding the mechanism of OP orientation lies in the in-situ characterization of the crystallization process during the drying of precursor solution. In-situ GIWAXS was applied for characterization of the crystallization process of RP perovskite deposited by hot-casting [64]. However, the crystallization process was still too fast to be observed.

3.2 In-plane orientation

For polycrystalline film, RT spin-coated $PentA_2MA_{n-1}Pb_nI_{3n+1}$ ($PentA^+$: pentylammonium) with IP orientation was obtained by adding tetrahydrothiophene-1-oxide (THTO) or DMSO into the precursor solution [68]. The IP orientation control by adding DMSO or THTO was suspected by forming the complexes of the sulfoxide group of DMSO or THTO with Pb^{2+} ions [68]. The complexes held the Pb^{2+} within the liquid phase and reduced the crystallization process where Pb^{2+} was locked in the OP oriented QWs by bonding with MA^+. Since the single crystal grows along QWs direction, the IP oriented RP perovskite can be obtained by mechanical exfoliation method on target substrates. As a widely-applied technique in 2D materials researches, the mechanical exfoliation is also available for the formation of ultrathin BA_2PbI_4 and PEA_2PbI_4 sheets [69, 70]. However, the 2D perovskite sheet formed by this method is low-productive and hard to control the layer number of the exfoliated RP perovskite, and so that directly forming 2D perovskite with in-plane orientation by solution method is worth to pursue. By solution method, atomically thin 2D BA_2PbBr_4 crystals ($\sim$ 1.6 nm thickness, 1–10 μm lateral size) can be formed by controlling the crystallization with a ternary solvent: dimethylformamide (DMF) chlorobenzene (CB) and acetonitrile (ACN) [42]. In the ternary solvent, DMF facilitates the dissolution of the precursors. CB helps to adjust the solubility of precursors in DMF. The acetonitrile has a higher vapor pressure and it leave the solution quickly under heating, it is used to balance the dissolution and crystallization of the 2D hybrid perovskites [42, 71]. Moreover, the -CN/-OH group in ACN is proposed to be adsorbed on specific polar crystal planes of perovskites during their self-assembly which further inhibited the *c*-axis growth of 2D perovskite sheets [71]. Furthermore, branched growth and large lateral sized 2D perovskite (up to $\sim$ 40 μm) BA_2PbBr_4 cross-stars sheets were obtained by slowing down the drying of the solvent [71]. Recently, a "induced peripheral crystallization" method was developed to grow multi-inch single-crystalline PEA_2PbI_4 perovskite membrane, which displayed ultralow defect density, long-term stability, and excellent flexibility [72].

Besides one-step solution methods, 2D perovskite nanosheets can also be obtained by reacting lead halide nanosheets with methylammonium halide (MAX) vapor. Here we involve the formation of ultra-thin perovskite sheets without bulky ammonium cations (steric effects) into discussion, although there is not organic spacing inserted between adjacent 2D perovskite sheets. In Fig. 3(e), a two-step vapor-phase method for the formation of methyl ammonium halide nanoplatelets ($MA_{n+1}Pb_nX_{3n+1}$) was illustrated. $MA_{n+1}Pb_nX_{3n}$ nanoplates was synthesized by first van der Waals (VDW) epitaxy of PbX_2 nanoplates and then converting the PbI_2 nanoplates to $MA_{n+1}Pb_nX_{3n}$ in MAX vapor [73]. The resulting $MA_{n+1}Pb_nI_{3n+1}$ nanoplates were 70 nm thick with $n > 50$. Furthermore, if the thickness of PbI_2 was controlled within few atomic layers, quasi-2D perovskite ($MA_{n+1}Pb_nX_{3n+1}$) with larger lateral size can be fabricated. For example, by hot casting the PbI_2 solution for 2D PbI_2 nanosheets, single-layered MA_2PbI_4 nanosheets were fabricated after reacting the 2D PbI_2 nanosheets with MAI vapor [74]. Besides the two-step vapor-phase method, one-step vapor-phase method was further developed by co-evaporated the PbX_2 and MAX. For example, with $PbCl_2$ placed in the furnace heated at 360°–380° and MACl placed $\sim$ 6 cm away from $PbCl_2$ in the upper stream at its melting temperature, MACl and $PbCl_2$ were co-evaporated on the mica substrate and $MA_{n+1}Pb_nCl_{3n+1}$ nanoplate with a thickness of 8.7 nm and lateral dimension of over 20 μm was obtained [75]. Different morphologies of the $MA_{n+1}Pb_nCl_{3n+1}$ nanoplates were obtained at different locations from the precursor vapor. The growth rate was determined by the adatoms of VDW-type diffusion and anisotropic surface free energy of the perovskite film. At the initial stage of film growth, surface energy dominates and a square shape was formed. Then the anisotropy in the adatom-capturing capability of different sites at the film edges resulted in a ⟨110⟩ fractal growth [75]. The perfect in-plane orientation of perovskite nanoplates by vapor-phase method showed promising application for field effect transistors [74]. Moreover, it is found that the PbI_2 crystal preferred to epitaxial grow on the other 2D materials such as graphene, hexagonal boron nitride (h-BN), and molybdenum disulfide (MoS_2), when these 2D materials located separately on SiO_2/Si substrate [76]. After conversion of the PbI_2 to 2D perovskite via vapor method, 2D perovskite/inorganic 2D materials heterojunctions were formed, which showed promising potentials for the application combined with inorganic 2D materials [76, 77]. In addition, combined the ternary solvent method processed single-layered RP perovskite nanoplates with the vapor-phase method, in-plane orientated RP perovskite $BA_2MA_{n-1}Pb_nBr_{3n+1}$ nanoplates could be obtained by reacting in-plane orientated BA_2PbBr_4 nanoplate with MABr vapor [78]. As shown in Fig. 3(f), the reaction of BA_2PbBr_4 nanoplate and MABr took place by interca-

lation of MABr between the layers and excluding BABr at 120°, in which the layer number n to be tuneable by reaction time [78].

4 Phase separation

For polycrystalline RP perovskite film, the result film was composed of RP perovskite with different layer number n, thus we defined $\langle n \rangle$ as the average n that determined by the composition in precursor solution. The phase separation between RP with different layer number in polycrystalline $BA_2MA_{n-1}Pb_nI_{3n+1}$RP perovskite film prepared by hot-casting can be detected by steady state PL and transient absorption (TA) spectra as shown in Figs. 4(a)–(c) [79]. When the perovskite film was illuminated from bottom side, exciton emission peaks of small-n ($n = 2, 3, 4$, peaks at $\sim$ 572, 608, and 645 nm, respectively) and large-n ($n \approx \infty$, at $\sim$ 750 nm) RP perovskites were observed. However, when the perovskite film was illuminated from top side, emission peak of large-n ($\sim$ 750 nm) RP perovskite dominated. This indicated that the large-n and small-n RP perovskite phase preferred to locate at the surface and the bottom of the RP perovskite film, respectively. Moreover, the separation between large-n and small-n RP perovskite phases can be identified from TA results [80]. Moreover, it was found that the absorption bleaching of large-n RP perovskite phase raised along with the decay of absorption bleaching of small-n RP perovskite [79]. This indicated that there is a phase separation in resulted RP perovskite film with a scale level of carrier diffusion length or even energy transfer length, so that considerable electrons transferred from small-n RP perovskite to large-n RP perovskite. Remarkably, the phase separation was directly observed with high-resolution TEM and position-resolved absorption spectra recently [81], in that study, both vertical and lateral phase segregation were observed. The formation of the phase separation is explained by the prior precipitation of quasi-3D perovskite, which resulted in the vertical phase segregation, and regional fast growth of 2D perovskite, which explained the lateral phase segregation. Based on this observation, energy transfer from 2D perovskite to quasi-3D perovskite was proposed, where after energy transfer, excitons were

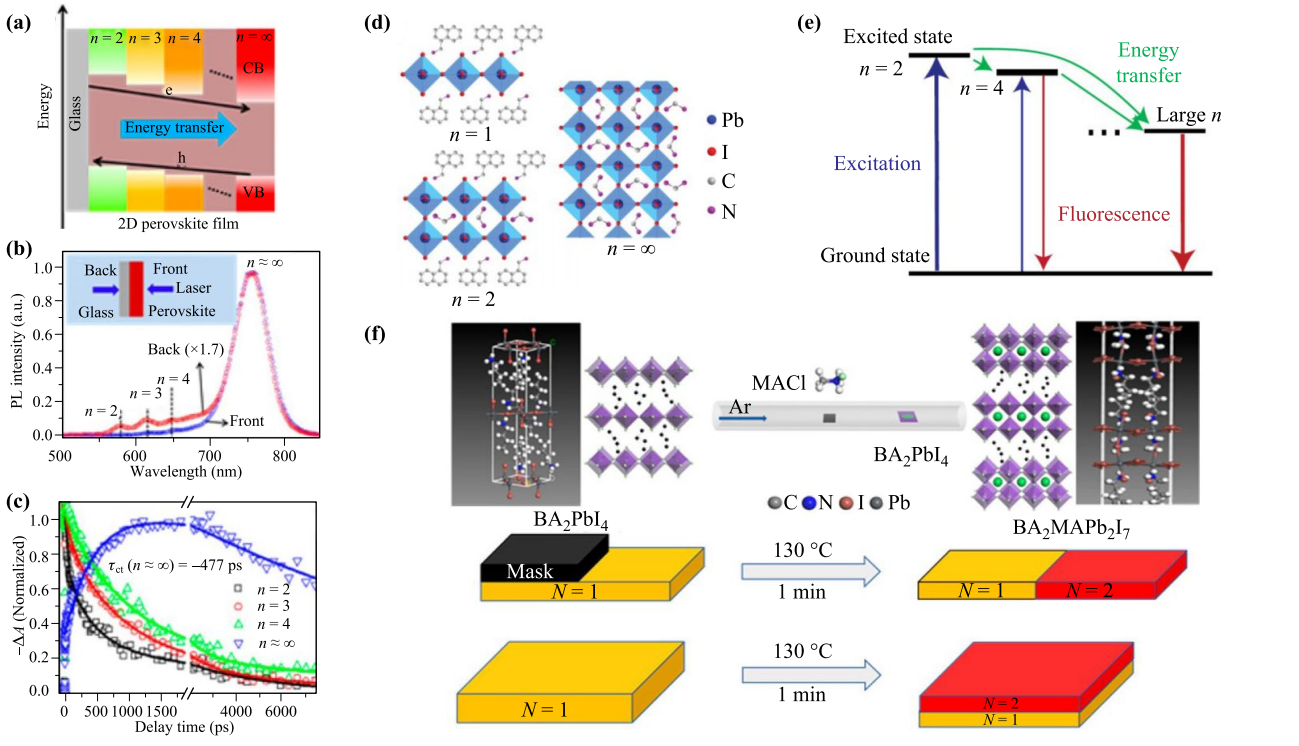

Fig. 4 **(a)** Comparative bandgap energy alignment of $BA_2MA_{n-1}Pb_nI_{3n+1}$ perovskites with different n values and three possible carrier transfer mechanisms: electron and energy transfers from small-n to large-n perovskites and hole transfer from large-n to small-n perovskites. **(b)** PL spectra of $BA_2MA_3Pb_4I_{13}$ perovskite film by hot-casting method illuminated from the front and back sides by a 405 nm laser. **(c)** Femtosecond transient absorption (TA) kinetics probed at $n = 2, 3, 4$ and $n \approx \infty$ bands under back-excitation. a, b and c were reproduced with permission from Ref. [79], Copyright © 2017 American Chemical Society. **(d, e)** Scheme of $NMA_2MA_{n-1}Pb_nI_{3n+1}$ (NMA: 1-naphthylmethylamine) and cascade energy transfer from smaller-n quantum wells (QWs) to larger-n QWs. d, e were reproduced with permission from Ref. [82], Copyright © 2016 Springer Nature. **(f)** Scheme of the gas-solid phase intercalation process to synthesize the lateral and vertical heterostructures with $BA_2PbI_4/BA_2MAPb_2I_7$. Reproduced with permission from Ref. [86], Copyright © 2017 American Chemical Society.

generated in quasi-3D perovskites, which would dissociate into free charges quickly due to the very small exciton binding energy in 3D-like perovskites. Since the exciton binding energy in 2D perovskites is much larger than thermal energy at room temperature, the energy transfer process may explain the effective exciton dissociation in 2D perovskite film.

The phase separation impact a lot on the working process of RP perovskite based solar cells and light emitting diodes [58, 82, 83]. Both energy transfer and charge transfer between large-n and small-n RP perovskite phases have been investigated by many groups [58, 79, 82–85]. The charge transfer process was proposed in $BA_2MA_{n-1}Pb_nI_{3n+1}$ film by applying electron or hole transfer materials [58, 79]. When electron transfer materials (ETM) covered on the top of RP perovskite film, the electrons of large-n RP perovskite further transferred electrons to ETM, resulting the disappearance of photobleaching (PB) raising of large-n RP perovskite. When the hole transfer materials (HTM) was covered on the top, the photobleaching (PB) raising of large-n RP perovskite remains, indicating the holes generated of the small-n RP perovskite cannot diffuse to the top large-n RP perovskite [58, 79]. Moreover, contrast to the PB raising, time-resolved PL of large-n RP perovskite decayed at the beginning, suggested the charge transfer process in $BA_2MA_{n-1}Pb_nI_{3n+1}$ film [79]. The charge transfer process between BA-based RP perovskite phase was also observed in ref. [84], where vertical phase separation was achieved by spin-coating BAI on top of $MAPbI_3$ film. Moreover, the charge transfer process also applied to $PEA_2MA_{n-1}Pb_nI_{3n+1}$ perovskite [58, 85]. On the other hand, the energy transfer process is also proposed as an important process for the efficient charge collection in RP perovskite based solar cells. The energy transfer process with both electrons and holes transferred from small-n RP perovskite to large-n RP perovskite [as shown in Figs. 4(d) and (e)] was also utilized in the field of perovskite LEDs [82, 83]. The cascade energy transfer of photon excitation for small-n RP perovskites to large-n RP perovskite was revealed by observation of the fast and slow exciton localization time of large-n RP perovskite [82]. The energy transfer process was also revealed for IP orientated $PEA_2MA_{n-1}Pb_nI_{3n+1}$ film by TA and time-resolved PL spectra. The PL decay from small-n exhibited a bi-exponential behavior with the fast decay attributed to a carrier funneling process [83]. At last, to demonstrate precisely controlled phase separation, an example of lateral and vertical phase separation with $n = 1/n = 2$ heterostructures was shown in Fig. 4(f) [86]. For both vertical and lateral heterostructures, centimeter-size BA_2PbI_4 (BA_2PbBr_4 and PEA_2PbI_4) plates was placed at the downstream of the quartz tube and reacted with the MACl or MAI vapor blown from upstream. For the synthesis of the lateral heterostructures, the as-grown $n = 1$ plate was partially covered by using a shadow mask [86].

5 Formation of 2D perovskite crystals on 3D perovskites surface

To avoid the trade-off between efficiency and stability when 2D perovskites were adopted as absorbers in solar cells, strategies of combining 2D perovskites with 3D perovskites while maintaining the structural integrity of the two phases were proposed [87–90].

The first strategy is ion exchange by spin coating A′X/isopropanol [91] on the top of 3D perovskite where long cations such as BA^+ [92], iso-butylammonium [93], octylammonium [92], cyclopropylammonium [94], PEA^+ [95–97], 5-aminovaleric acid [98], $NH_3(CH_2)_4NH_3^{2+}$ [99], $NH_3(CH_2)_2O(CH_2)_2NH_3^{2+}$ [99], $NH_3(CH_2)_8NH_3^{2+}$ [99], tetra-methyl ammonium [34], hexadecyl trimethyl ammonium [34], tetra-ethyl ammonium [34], tetra-butyl ammonium [34] and tetra-hexyl ammonium [34] were investigated. In addition, A′X could also be added into anti-solvent to achieve graded 3D–2D halide perovskite interface [100]. As a common method for fabricating 3D perovskite film, antisolvent was dropped on the film during spin-coating process to induce fast crystallization of 3D perovskite [101, 102]. When antisolvent with PEAI was dropped on the film, some PEA^+ remained on the surface, resulting a gradually increased concentration of 2D perovskite from bottom to top. The 2D perovskite on the top has a higher conductive band level and disfavors the interface recombination [103], resulting an improved open circuit voltage (Voc) and PCE of the solar cells [100]. Besides the ion exchange, the A′X could also react with the remnant PbI_2 to achieve passivation effect [104, 105]. The remnant PbI_2, which was formed by over annealing or by adding excess ratio of PbI_2 in precursor solution, was found to locate at the 3D perovskite grain boundaries and at the interfaces between 3D perovskite layer and ETM or HTM layer [106–110]. The capping PbI_2 formed type I band gap alignment with the inner 3D perovskite and suppressed the interface defect trapping [107, 110]. However, the perovskite film with remnant PbI_2 showed poorer stability against illumination and humidity [111]. Therefore, by spin-coating guanidinium bromide (GABr) or PEAI solution on top of PbI_2 capped 3D perovskite, the capping PbI_2 can be transferred to capping 2D perovskite, in which way, the passivation effect was retained while the stability against illumination and humidity was improved [104, 105]. Similar to ion-exchange passivation method, n-butylamine [112], aniline [113], benzylamine [113] and phenethylamine [113] diluted in chlorobenzene could be spin-coated on the 3D perovskite surface to induce the reaction of $2BA + MAI + MAPbI_3 \rightarrow BA_2PbI_4 + 2MA\uparrow$ for BA case.

When small ratio of 2D perovskite was added into 3D perovskite precursor solution, the 2D perovskite was found to spontaneously crystallize at the boundaries of the 3D perovskite grain or between grains [62, 114]. For example,

when PEA_2PbI_4 was added into $FAPbI_3$ perovskite precursor solution, the formed capping PEA_2PbI_4 protected the $FAPbI_3$ perovskite from moisture and suppress ion migration [114]. When BA^+ cations were introduced into $FA_{0.83}Cs_{0.17}Pb(I_yBr_{1-y})_3$ 3D perovskite, 2D perovskite platelets between highly (h00) orientated 3D perovskite grains were formed [62].

6 Impact of 2D perovskites on phase/device stability

Due to the hydrophobic nature of long cation ions, the stability against moisture was much improved for RP perovskite than 3D perovskite [35, 36]. As shown in Figs. 5(c) and (d), after 2-month storage at 40% relative humidity environment, while $MAPbI_3$ decayed to PbI_2, no PbI_2 XRD peak and color change was observed for RR perovskite film, which indicated the better stability of RP perovskite than 3D perovskite. The improved device stability again moisture was demonstrated after applying hydrophobic cations $(CF_3)_3CO(CH_2)_3NH_3^+$ and $C_6H_2F_3NH_3^+$ for solar cells [115] and LEDs [116], respectively. Moreover, the improved stability against humidity was also demonstrated for 2D passivated 3D perovskite film [34]. Using in situ neutron and X-ray scattering techniques, rapid disproportionation of the initial 2D phase ($n = 5$ on top of $MAPbI_3$) into lower-n phases under humidity was observed, which further suppressed the escape of MAI, thus in turn improved the stability of the film against moisture [117]. Apart from hydrophobicity of long-chain cation, since MAI can decompose into volatile MA gas and HI [118], the better thermal stability of long-chain iodide cation than MA might also contribute to the improved overall stability.

In addition, the frequently observed ion migration problem is one of the important factors for current–voltage hysteresis and structural instability of perovskites [119–121]. Noticeably, suppressed ion migration along both OP and IP directions in RP perovskite have been demonstrated, which might be due to the blocking effect of long-chain cations or the lower density of vacancies [122, 123]. The suppressed ion migration and the protecting effect of the long-chain cation in turn provides much improved stability of photovoltaic device against moisture and sun illumination [48, 114].

Noting that $FAPbI_3$ and $CsPbI_3$ were more stable at hexagonal and orthorhombic phase, respectively [124]. However, both two phases are unfavorable for solar cells application due to their large bandgap. Therefore, 2D per-

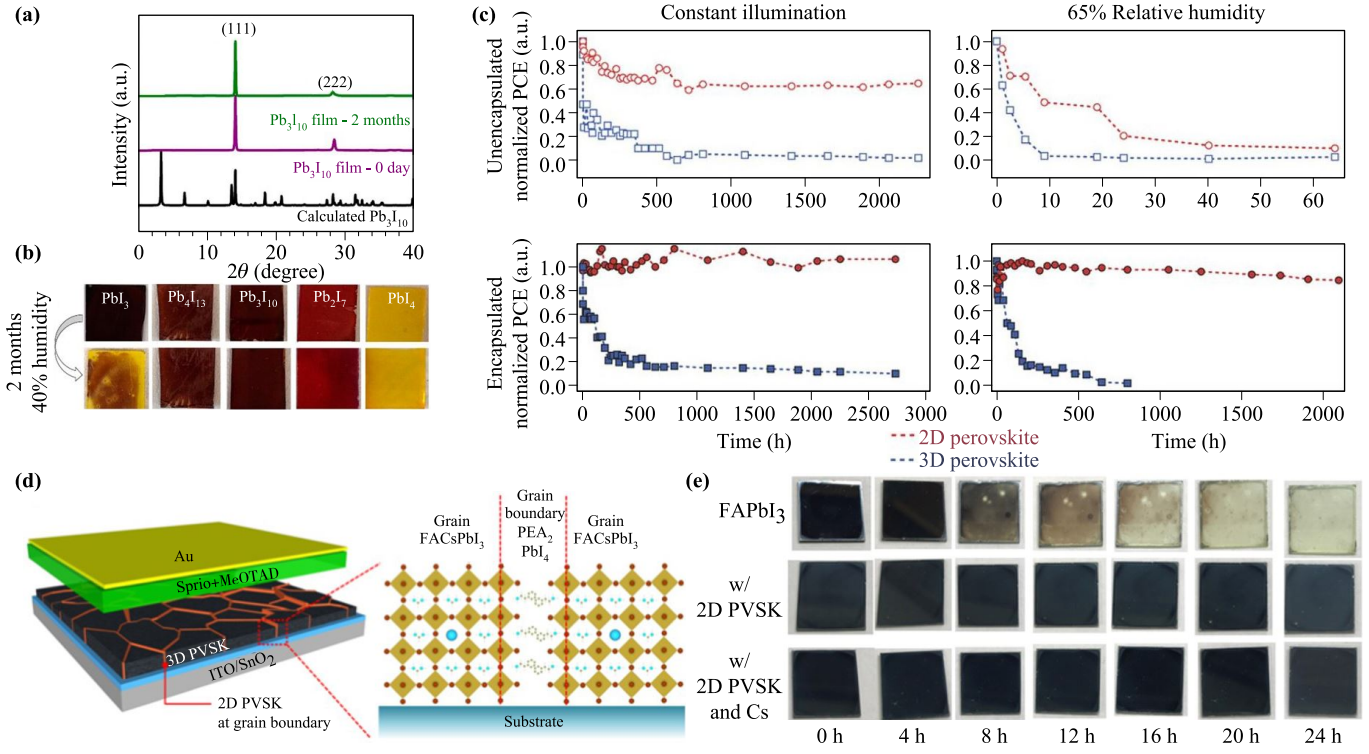

Fig. 5 **(a, b)** XRD patterns and photos showing the improved stability against moisture of $BA_2MA_{n-1}Pb_nI_{3n+1}$ ($n = 1$–4) compared with $MAPbI_3$. Reproduced with permission from Ref. [36], Copyright © 2015 American Chemical Society. **(c)** Improved device stability of RP perovskite solar cells based on $BA_2MA_3Pb_4I_{13}$ compared with 3D perovskite solar cells based on $MAPbI_3$. Reproduced with permission from Ref. [48], Copyright © 2016 Springer Nature. **(d)** Scheme of $FAPbI_3$ passivated by PEA_2PbI_4. **(e)** Improved phase stability of $FAPbI_3$ with passivation of PEA_2PbI_4. d, e were reproduced with permission from Ref. [114], Copyright © 2018 Springer Nature.

ovskite were added into the 3D perovskite precursor solution to stabilize both $FAPbI_3$ and $CsPbI_3$ at the cubic phase [114, 125]. The mechanism to stabilize cubic phase was explained by improved cubic phase purity at formation stage of perovskite film or by the reduced grain size for $FAPbI_3$ [114] [as shown in Figs. 5(a), (b)] and $CsPbI_3$ [125], respectively.

7 Controlled nanostructure

RP perovskite with nanostructures is favored in the development of perovskite light emitting devices [126–128], solar cells [129, 130], photodetector [131, 132] or lasing [133, 134]. To control the shape of the nanocrystals (NCs), solvent-induced reprecipitation method and ligand-assisted reprecipitation method were usually adopted. For solvent-induced reprecipitation method, octadecene was used as solvent and 3D perovskite precursor was reacted in octadecene with crystallization controlled by octylamine (OM) and oleic acid (OA). When reaction was usually quenched by adding acetone or by the ice-water bath. By this method, $MAPbBr_3$ perovskite NCs were synthesized by adding $PbBr_2$, MABr, and octylammonium bromide to a stirring solution of oleic acid and 1-octadecene at 80 °C, followed by quenching the reaction with acetone [135]. The resulting NCs contained both nanoparticles and nanoplatelets. The 2D perovskite nanoplatelets can be isolated by diluting the precipitation toluene and reprecipitated by adding acetone [135]. To control the shape of NCs and the unit cell number, the reaction temperature was modified. When the reaction temperature decreased from 150 ° to 90 °, the shape of $CsPbBr_3$ NCs changed from nanocubes to nanoplatelets [136]. The tunable shapes (nanocubes, nanowires, and nanoplatelets) of $CH_3NH_3PbX_3$ (X = Br or I) NCs was achieved by varying the ratio of OM to OA [137]. In general, OM controls the size of formed NCs, whereas oleic acid suppresses aggregation effects. Low reaction temperatures and high ligand concentrations always favor anisotropic growth, mainly producing nanoplatelets [138].

In ligand-assisted re-precipitation (LARP) method, the perovskite precursors with OM and OA in a good solvent (e.g., DMF or γ-butyrolactone) was injected into a bad solvent (e.g., toluene or acetone) [139, 140]. By tuning the amounts of OM and OA, the shapes of $CsPbBr_3$ NCs changed from lamellar-structured 0D quantum dots to face-to-face stacking 2D nanoplatelets and flat-lying 2D nanosheets as shown in Fig. 6(a) [141]. Similarly, $MAPbBr_3$ nanoplatelets were synthesized by LARP method, with tunable atomic layer numbers obtained by adding different amount of octylammonium bromide [142]. Besides ratio of OM and OA, the shape of nanostructure could also be modified by applying different types of organic acid and amine ligands [143]. When OM and OA were adding in the bad solvent (i.e., toluene) instead of precursor solution, $MAPbBr_3$ nanoplatelets were also formed with atomic layer controlled by the amount of OM and OA [44].

Apart from the shape control of nanostructure by direct synthesis, the perovskite nanoplatelets can also be obtained by diluting microcrystals solution in toluene with octylamine [144, 145]. The thickness of the nanoplatelets can be controlled both by the dilution level and by the ligand concentration as shown in Fig. 6(b). The shape change from large NCs to nanoplatelet was explained by osmotic

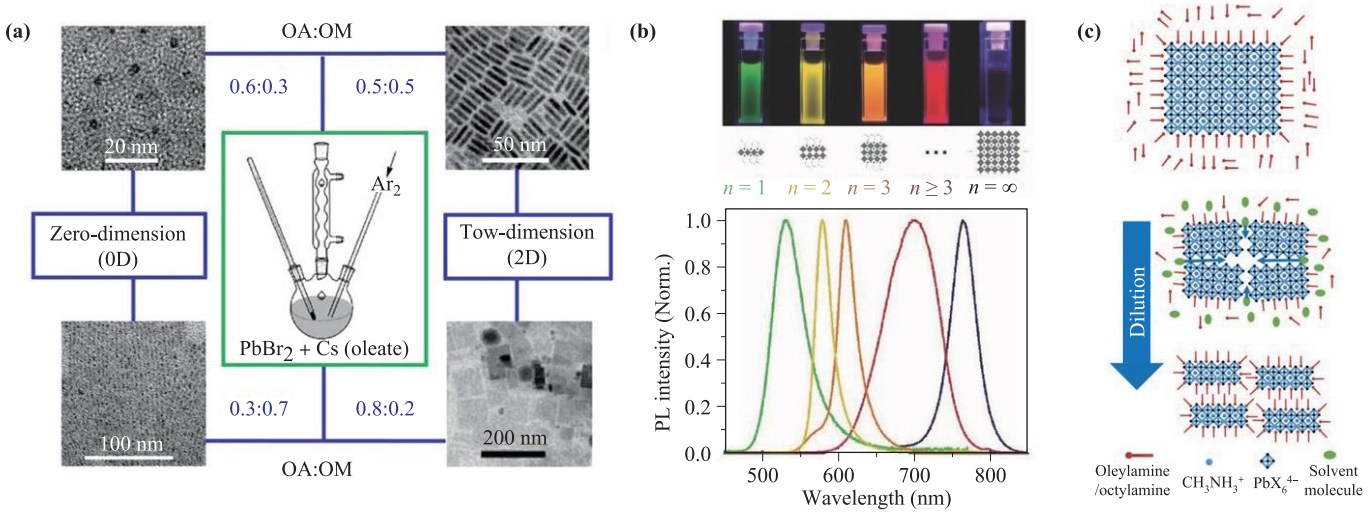

Fig. 6 **(a)** $CsPbBr_3$ NCs with various shapes by LARP method with different ratio of OA and OM. Reproduced with permission from Ref. [141], Copyright © 2016 American Chemical Society. **(b)** $MAPbI_3$ nanoplates prepared by diluting large $MAPbI_3$ microcrystals solution in toluene with octylamine. Reproduced with permission from Ref. [144], Copyright © 2016 John Wiley and Sons. **(c)** Schematic of the dilution-induced fragmentation of perovskite microcrystals into nanoplates. Reproduced with permission from Ref. [145], Copyright © 2016 American Chemical Society.

swelling of large NCs along with the quick passivation of organic ligands as shown in Fig. 6(c) [145].

8 Prospects

In conclusion, atomic structure and crystal control of 2D perovskite were reviewed. Despite the excellent works done to control the formation of 2D perovskites for optoelectronic device, some open questions still remain and new strategies continue to emerge. First, exploring multifunctional long-chain cations for RP perovskite may pave another way for developing high efficient optoelectronic device. For example, long cations with high dipole moment might promote separation of photo-generated electron–hole pairs and suppress nonradiative recombination by reducing exciton binding energy, which resulted in an improved PCE of perovskite solar cells. Applying cations with better hydrophobic property might further improve the stability of RP perovskite against humidity. Second, a clear understanding of the mechanism about OP orientation would benefit developing RP perovskite solar cells with higher efficiency. Up to now, the PCEs of RP perovskite solar cells still lagged behind the 3D perovskite solar cells. One of the reasons lies in the misalignment of vertically packed quantum wells. Therefore, better crystallization along OP direction would favor charge transport and improve the performance of RP perovskite solar cells. Third, since single crystals with less traps would enable a high charge mobility, devices based on RP perovskite single crystals might show a better performance than the devices based on polycrystalline film. However, except single-crystalline PEA_2PbI_4 perovskite membrane was fabricated, reports on large-size RP single crystals is still sparse.

Acknowledgements We thank the financial support from the National Natural Science Foundation of China (Grant No. 51673218), the Open Fund of the State Key Laboratory of Integrated Optoelectronics (IOSKL2016KF05), and the Central South University Postdoctoral International Exchange Introduction Program, China Postdoctoral Science Foundation.

References

1. H. R. Wenk and A. Bulakh, Minerals: Their Constitution and Origin, Cambridge University Press, Cambridge, 2004
2. C. K. Møller, Crystal structure and photoconductivity of cæsium plumbohalides, *Nature* 182(4647), 1436 (1958)
3. D. Weber, $CH_3NH_3PbX_3$, ein Pb(II)-System mit kubischer Perowskitstruktur/$CH_3NH_3PbX_3$, a Pb(II)-System with Cubic Perovskite Structure, *Z. Naturforsch. B* 33(12), 1443 (1978)
4. D. B. Mitzi, C. A. Feild, W. T. A. Harrison, and A. M. Guloy, Conducting tin halides with a layered organic-based perovskite structure, *Nature* 369(6480), 467 (1994)
5. C. R. Kagan, D. B. Mitzi, and C. D. Dimitrakopoulos, Organic-inorganic hybrid materials as semiconducting channels in thin-film field-effect transistors, *Science* 286(5441), 945 (1999)
6. D. B. Mitzi, K. Chondroudis, and C. R. Kagan, Organic-inorganic electronics, *IBM J. Res. Develop.* 45(1), 29 (2001)
7. A. Kojima, K. Teshima, Y. Shirai, and T. Miyasaka, Organometal halide perovskites as visible-light sensitizers for photovoltaic cells, *J. Am. Chem. Soc.* 131(17), 6050 (2009)
8. G. E. Eperon, S. D. Stranks, C. Menelaou, M. B. Johnston, L. M. Herz, and H. J. Snaith, Formamidinium lead trihalide: a broadly tunable perovskite for efficient planar heterojunction solar cells, *Energy Environ. Sci.* 7(3), 982 (2014)
9. Z. Fan, K. Sun, and J. Wang, Perovskites for photovoltaics: A combined review of organic-inorganic halide perovskites and ferroelectric oxide perovskites, *J. Mater. Chem. A* 3(37), 18809 (2015)
10. C. Zhou, H. Lin, Q. He, L. Xu, M. Worku, M. Chaaban, S. Lee, X. Shi, M. H. Du, and B. Ma, Low dimensional metal halide perovskites and hybrids, *Mater. Sci. Eng. Rep.* 137, 38 (2019)
11. H. Lin, C. Zhou, Y. Tian, T. Siegrist, and B. Ma, Low-dimensional organometal halide perovskites, *ACS Energy Lett.* 3(1), 54 (2018)
12. B. Saparov and D. B. Mitzi, Organic–inorganic perovskites: Structural versatility for functional materials design, *Chem. Rev.* 116(7), 4558 (2016)
13. L. Mao, C. C. Stoumpos, and M. G. Kanatzidis, Two-dimensional hybrid halide perovskites: Principles and promises, *J. Am. Chem. Soc.* 141(3), 1171 (2019)
14. X. Li, J. Hoffman, W. Ke, M. Chen, H. Tsai, W. Nie, A. D. Mohite, M. Kepenekian, C. Katan, J. Even, M. R. Wasielewski, C. C. Stoumpos, and M. G. Kanatzidis, Two-dimensional halide perovskites incorporating straight chain symmetric diammonium ions, $(NH_3C_mH_{2m}NH_3)$ $(CH_3NH_3)_{n-1}PbnI_{3n+1}$ ($m = 4$–9; $n = 1$–4), *J. Am. Chem. Soc.* 140(38), 12226 (2018)
15. K. Lin, J. Xing, L. N. Quan, F. P. G. de Arquer, X. Gong, J. Lu, L. Xie, W. Zhao, D. Zhang, C. Yan, W. Li, X. Liu, Y. Lu, J. Kirman, E. H. Sargent, Q. Xiong, and Z. Wei, Perovskite light-emitting diodes with external quantum efficiency exceeding 20 per cent, *Nature* 562(7726), 245 (2018)
16. Y. Cao, N. Wang, H. Tian, J. Guo, Y. Wei, H. Chen, Y. Miao, W. Zou, K. Pan, Y. He, H. Cao, Y. Ke, M. Xu, Y. Wang, M. Yang, K. Du, Z. Fu, D. Kong, D. Dai, Y. Jin, G. Li, H. Li, Q. Peng, J. Wang, and W. Huang, Perovskite light-emitting diodes based on spontaneously formed submicrometre-scale structures, *Nature* 562(7726), 249 (2018)
17. J. Luo, X. Wang, S. Li, J. Liu, Y. Guo, G. Niu, L. Yao, Y. Fu, L. Gao, Q. Dong, C. Zhao, M. Leng, F. Ma, W. Liang, L. Wang, S. Jin, J. Han, L. Zhang, J. Etheridge, J.

Wang, Y. Yan, E. H. Sargent, and J. Tang, Efficient and stable emission of warm-white light from lead-free halide double perovskites, *Nature* 563(7732), 541 (2018)

18. L. Dou, Y. M. Yang, J. You, Z. Hong, W. H. Chang, G. Li, and Y. Yang, Solution-processed hybrid perovskite photodetectors with high detectivity, *Nat. Commun.* 5(1), 5404 (2014)

19. Y. J. Fang, Q. F. Dong, Y. C. Shao, Y. B. Yuan, and J. S. Huang, Highly narrowband perovskite single-crystal photodetectors enabled by surface-charge recombination, *Nat. Photonics* 9(10), 679 (2015)

20. S. Tong, J. Sun, C. Wang, Y. Huang, C. Zhang, J. Shen, H. Xie, D. Niu, S. Xiao, Y. Yuan, J. He, J. Yang, and Y. Gao, High-performance broadband perovskite photodetectors based on $CH_3NH_3PbI_3/C_8BTBT$ heterojunction, *Adv. Electron. Mater.* 3(7), 1700058 (2017)

21. H. Xia, S. Tong, C. Zhang, C. Wang, J. Sun, J. He, J. Zhang, Y. Gao, and J. Yang, Flexible and air-stable perovskite network photodetectors based on $CH_3NH_3PbI_3/C_8BTBT$ bulk heterojunction, *Appl. Phys. Lett.* 112(23), 233301 (2018)

22. S. Li, S. Tong, J. Q. Meng, C. Zhang, C. Zhang, J. Shen, S. Xiao, J. Sun, J. He, Y. Gao, B. Yang, and J. Yang, Fast-response and high-responsivity $FA_xMA_{1-x}PbI_3$ photodetectors fabricated via doctor-blading deposition in ambient condition, *Org. Electron.* 52, 190 (2018)

23. S. Tong, H. Wu, C. Zhang, S. Li, C. Wang, J. Shen, S. Xiao, J. He, J. Yang, J. Sun, and Y. Gao, Large-area and high-performance CH3NH3PbI3 perovskite photodetectors fabricated via doctor blading in ambient condition, *Org. Electron.* 49, 347 (2017)

24. W. Hu, R. Wu, S. Yang, P. Fan, J. Yang, and A. Pan, Solvent-induced crystallization for hybrid perovskite thin-film photodetector with high-performance and low working voltage, *J. Phys. D Appl. Phys.* 50(37), 375101 (2017)

25. W. Yu, F. Li, L. Yu, M. R. Niazi, Y. Zou, D. Corzo, A. Basu, C. Ma, S. Dey, M. L. Tietze, U. Buttner, X. Wang, Z. Wang, M. N. Hedhili, C. Guo, T. Wu, and A. Amassian, Single crystal hybrid perovskite field-effect transistors, *Nat. Commun.* 9(1), 5354 (2018)

26. X. Y. Chin, D. Cortecchia, J. Yin, A. Bruno, and C. Soci, Lead iodide perovskite light-emitting field-effect transistor, *Nat. Commun.* 6(1), 7383 (2015)

27. S. P. Senanayak, B. Yang, T. H. Thomas, N. Giesbrecht, W. Huang, E. Gann, B. Nair, K. Goedel, S. Guha, X. Moya, C. R. McNeill, P. Docampo, A. Sadhanala, R. H. Friend, and H. Sirringhaus, Understanding charge transport in lead iodide perovskite thin-film field-effect transistors, *Sci. Adv.* 3(1), e1601935 (2017)

28. X. Qi, Y. Zhang, Q. Ou, S. T. Ha, C. W. Qiu, H. Zhang, Y. B. Cheng, Q. Xiong, and Q. Bao, Photonics and optoelectronics of 2D metal-halide perovskites, *Small* 14(31), e1800682 (2018)

29. G. Liu, B. Yang, B. Liu, C. Zhang, S. Xiao, Y. Yuan, H. Xie, D. Niu, J. Yang, Y. Gao, and C. Zhou, Irreversible light-soaking effect of perovskite solar cells caused by light-induced oxygen vacancies in titanium oxide, *Appl. Phys. Lett.* 111(15), 153501 (2017)

30. F. Wan, X. Qiu, H. Chen, Y. Liu, H. Xie, J. Shi, H. Huang, Y. Yuan, Y. Gao, and C. Zhou, Accelerated electron extraction and improved UV stability of TiO_2 based perovskite solar cells by SnO_2 based surface passivation, *Org. Electron.* 59, 184 (2018)

31. C. Wang, C. Zhang, Y. Huang, S. Tong, H. Wu, J. Zhang, Y. Gao, and J. Yang, Degradation behavior of planar heterojunction $CH_3NH_3PbI_3$ perovskite solar cells, *Synth. Met.* 227, 43 (2017)

32. J. Xiong, B. Yang, C. Cao, R. Wu, Y. Huang, J. Sun, J. Zhang, C. Liu, S. Tao, Y. Gao, and J. Yang, Interface degradation of perovskite solar cells and its modification using an annealing-free TiO_2 NPs layer, *Org. Electron.* 30, 30 (2016)

33. L. N. Quan, M. Yuan, R. Comin, O. Voznyy, E. M. Beauregard, S. Hoogland, A. Buin, A. R. Kirmani, K. Zhao, A. Amassian, D. H. Kim, and E. H. Sargent, Ligand-stabilized reduced-dimensionality perovskites, *J. Am. Chem. Soc.* 138(8), 2649 (2016)

34. S. Yang, Y. Wang, P. R. Liu, Y. B. Cheng, H. J. Zhao, and H. G. Yang, Functionalization of perovskite thin films with moisture-tolerant molecules, *Nat. Energy* 1(2), 15016 (2016)

35. I. C. Smith, E. T. Hoke, D. Solis-Ibarra, M. D. McGehee, and H. I. Karunadasa, A layered hybrid perovskite solar-cell absorber with enhanced moisture stability, *Angew. Chem. Int. Ed. Engl.* 53(42), 11232 (2014)

36. D. H. Cao, C. C. Stoumpos, O. K. Farha, J. T. Hupp, and M. G. Kanatzidis, 2D homologous perovskites as light-absorbing materials for solar cell applications, *J. Am. Chem. Soc.* 137(24), 7843 (2015)

37. C. C. Stoumpos, D. H. Cao, D. J. Clark, J. Young, J. M. Rondinelli, J. I. Jang, J. T. Hupp, and M. G. Kanatzidis, Ruddlesden–popper hybrid lead iodide perovskite 2D homologous semiconductors, *Chem. Mater.* 28(8), 2852 (2016)

38. L. Zhang, Y. Liu, Z. Yang, and S. Liu, Two dimensional metal halide perovskites: Promising candidates for light-emitting diodes, *J. Energy Chem.* 37, 97 (2019)

39. I. Borriello, G. Cantele, and D. Ninno, Ab initio investigation of hybrid organic-inorganic perovskites based on tin halides, *Phys. Rev. B* 77(23), 235214 (2008)

40. W. J. Yin, T. Shi, and Y. Yan, Unique properties of halide perovskites as possible origins of the superior solar cell performance, *Adv. Mater.* 26(27), 4653 (2014)

41. Y. Fu, H. Zhu, J. Chen, M. P. Hautzinger, X. Y. Zhu, and S. Jin, Metal halide perovskite nanostructures for optoelectronic applications and the study of physical properties, *Nat. Rev. Mater.* 4(3), 169 (2019)

42. L. Dou, A. B. Wong, Y. Yu, M. Lai, N. Kornienko, S. W. Eaton, A. Fu, C. G. Bischak, J. Ma, T. Ding, N. S. Ginsberg, L. W. Wang, A. P. Alivisatos, and P. Yang, Atomically thin two-dimensional organic-inorganic hybrid perovskites, *Science* 349(6255), 1518 (2015)

43. Z. Chen, C. Zhang, X. F. Jiang, M. Liu, R. Xia, T. Shi, D. Chen, Q. Xue, Y. J. Zhao, S. Su, H. L. Yip, and Y. Cao, High-performance color-tunable perovskite light emitting devices through structural modulation from bulk to layered film, *Adv. Mater.* 29(8), 1603157 (2017)

44. S. Kumar, J. Jagielski, S. Yakunin, P. Rice, Y. C. Chiu, M. Wang, G. Nedelcu, Y. Kim, S. Lin, E. J. G. Santos, M. V. Kovalenko, and C. J. Shih, Efficient blue electroluminescence using quantum-confined two-dimensional perovskites, *ACS Nano* 10(10), 9720 (2016)

45. M. C. Weidman, M. Seitz, S. D. Stranks, and W. A. Tisdale, Highly tunable colloidal perovskite nanoplatelets through variable cation, metal, and halide composition, *ACS Nano* 10(8), 7830 (2016)

46. S. Tan, N. Zhou, Y. Chen, L. Li, G. Liu, P. Liu, C. Zhu, J. Lu, W. Sun, Q. Chen, and H. Zhou, Effect of high dipole moment cation on layered 2D organic–inorganic halide perovskite solar cells, *Adv. Energy Mater.* 9(5), 1803024 (2019)

47. C. Ma, D. Shen, T. W. Ng, M. F. Lo, and C.S. Lee, 2D perovskites with short interlayer distance for high-performance solar cell application, *Adv. Mater.* 30(22), e1800710 (2018)

48. H. Tsai, W. Nie, J. C. Blancon, C. C. Stoumpos, R. Asadpour, B. Harutyunyan, A. J. Neukirch, R. Verduzco, J. J. Crochet, S. Tretiak, L. Pedesseau, J. Even, M. A. Alam, G. Gupta, J. Lou, P. M. Ajayan, M. J. Bedzyk, M. G. Kanatzidis, and A. D. Mohite, High-efficiency two-dimensional Ruddlesden–Popper perovskite solar cells, *Nature* 536(7616), 312 (2016)

49. A. Z. Chen, M. Shiu, J. H. Ma, M. R. Alpert, D. Zhang, B. J. Foley, D. M. Smilgies, S. H. Lee, and J. J. Choi, Origin of vertical orientation in two-dimensional metal halide perovskites and its effect on photovoltaic performance, *Nat. Commun.* 9(1), 1336 (2018)

50. H. Tsai, R. Asadpour, J. C. Blancon, C. C. Stoumpos, J. Even, P. M. Ajayan, M. G. Kanatzidis, M. A. Alam, A. D. Mohite, and W. Nie, Design principles for electronic charge transport in solution-processed vertically stacked 2D perovskite quantum wells, *Nat. Commun.* 9(1), 2130 (2018)

51. N. Zhou, Y. Shen, L. Li, S. Tan, N. Liu, G. Zheng, Q. Chen, and H. Zhou, Exploration of crystallization kinetics in quasi two-dimensional perovskite and high performance solar cells, *J. Am. Chem. Soc.* 140(1), 459 (2018)

52. X. Zhang, X. D. Ren, B. Liu, R. Munir, X. J. Zhu, D. Yang, J. B. Li, Y. C. Liu, D. M. Smilgies, R. P. Li, Z. Yang, T. Q. Niu, X. L. Wang, A. Amassian, K. Zhao, and S. Z. F. Liu, Stable high efficiency two-dimensional perovskite solar cells via cesium doping, *Energy Environ. Sci.* 10(10), 2095 (2017)

53. L. Mao, W. Ke, L. Pedesseau, Y. Wu, C. Katan, J. Even, M. R. Wasielewski, C. C. Stoumpos, and M. G. Kanatzidis, Hybrid Dion-Jacobson 2D lead iodide perovskites, *J. Am. Chem. Soc.* 140(10), 3775 (2018)

54. Y. N. Chen, Y. Sun, J. J. Peng, W. Zhang, X. J. Su, K. B. Zheng, T. Pullerits, and Z. Q. Liang, Tailoring organic cation of 2D Air-Stable Organometal Halide Perovskites for Highly Efficient Planar Solar Cells, *Adv. Energy Mater.* 7(18), 1700162 (2017)

55. X. Q. Zhang, G. Wu, W. F. Fu, M. C. Qin, W. T. Yang, J. L. Yan, Z. Q. Zhang, X. H. Lu, and H. Z. Chen, Orientation regulation of phenylethylammonium cation based 2D perovskite solar cell with efficiency higher than 11%, *Adv. Energy Mater.* 8(14), 1702498 (2018)

56. W. F. Fu, J. Wang, L. J. Zuo, K. Gao, F. Liu, D. S. Ginger, and A. K. Y. Jen, Two-dimensional perovskite solar cells with 14.1% power conversion efficiency and 0.68% external radiative efficiency, *ACS Energy Lett.* 3(9), 2086 (2018)

57. X. Zhang, G. Wu, S. Yang, W. Fu, Z. Zhang, C. Chen, W. Liu, J. Yan, W. Yang, and H. Chen, Vertically oriented 2D layered perovskite solar cells with enhanced efficiency and good stability, *Small* 13(33), 1700611 (2017)

58. J. Qing, X. K. Liu, M. J. Li, F. Liu, Z. C. Yuan, E. Tiukalova, Z. B. Yan, M. Duchamp, S. Chen, Y. M. Wang, S. Bai, J. M. Liu, H. J. Snaith, C. S. Lee, T. C. Sum, and F. Gao, Aligned and graded type-II Ruddlesden-Popper perovskite films for efficient solar cells, *Adv. Energy Mater.* 8(21), 1800185 (2018)

59. H. Lai, B. Kan, T. Liu, N. Zheng, Z. Xie, T. Zhou, X. Wan, X. Zhang, Y. Liu, and Y. Chen, Two-dimensional Ruddlesden-Popper perovskite with nanorod-like morphology for solar cells with efficiency exceeding 15%, *J. Am. Chem. Soc.* 140(37), 11639 (2018)

60. J. Chen, X. Lian, Y. Zhang, W. Yang, J. Li, M. Qin, X. Lu, G. Wu, and H. Chen, Interfacial engineering enables high efficiency with a high open-circuit voltage above 1.23 V in 2D perovskite solar cells, *J. Mater. Chem. A* 6(37), 18010 (2018)

61. J. Qiu, Y. Zheng, Y. Xia, L. Chao, Y. Chen, and W. Huang, Rapid crystallization for efficient 2D Ruddlesden–Popper (2DRP) perovskite solar cells, *Adv. Funct. Mater.* 0(0), 1806831 (2018)

62. Z. Wang, Q. Lin, F. P. Chmiel, N. Sakai, L. M. Herz, and H. J. Snaith, Efficient ambient-air-stable solar cells with 2D–3D heterostructured butylammonium-caesium-formamidinium lead halide perovskites, *Nat. Energy* 2(9), 17135 (2017)

63. C. M. M. Soe, W. Nie, C. C. Stoumpos, H. Tsai, J. C. Blancon, F. Liu, J. Even, T. J. Marks, A. D. Mohite, and M. G. Kanatzidis, Understanding film formation morphology and orientation in high member 2D Ruddlesden-Popper perovskites for high-efficiency solar cells, *Adv. Energy Mater.* 8(1), 1700979 (2018)

64. X. Zhang, R. Munir, Z. Xu, Y. Liu, H. Tsai, W. Nie, J. Li, T. Niu, D. M. Smilgies, M. G. Kanatzidis, A. D. Mohite, K. Zhao, A. Amassian, and S. F. Liu, Phase transition control for high performance Ruddlesden-Popper perovskite solar cells, *Adv. Mater.* 30(21), e1707166 (2018)

65. C. Zuo, A. D. Scully, D. Vak, W. Tan, X. Jiao, C. R. McNeill, D. Angmo, L. Ding, and M. Gao, Self-assembled 2D perovskite layers for efficient printable solar cells, *Adv. Energy Mater.* 9(4), 1803258 (2019)

66. R. Yang, R. Li, Y. Cao, Y. Wei, Y. Miao, W. L. Tan, X. Jiao, H. Chen, L. Zhang, Q. Chen, H. Zhang, W. Zou, Y. Wang, M. Yang, C. Yi, N. Wang, F. Gao, C. R. McNeill, T. Qin, J. Wang, and W. Huang, Oriented quasi-2D perovskites for high performance optoelectronic devices, *Adv. Mater.* 30(51), e1804771 (2018)
67. A. Z. Chen, M. Shiu, X. Deng, M. Mahmoud, D. Zhang, B. J. Foley, S. H. Lee, G. Giri, and J. J. Choi, Understanding the formation of vertical orientation in two-dimensional metal halide perovskite thin films, *Chem. Mater.* 31(4), 1336 (2019)
68. Y. H. Hu, L. M. Spies, D. Alonso-Alvarez, P. Mocherla, H. Jones, J. Hanisch, T. Bein, P. R. F. Barnes, and P. Docampo, Identifying and controlling phase purity in 2D hybrid perovskite thin films, *J. Mater. Chem. A* 6(44), 22215 (2018)
69. W. Niu, A. Eiden, G. V. Prakash, and J. J. Baumberg, Exfoliation of self-assembled 2D organic-inorganic perovskite semiconductors, *Appl. Phys. Lett.* 104(17), 171111 (2014)
70. O. Yaffe, A. Chernikov, Z. M. Norman, Y. Zhong, A. Velauthapillai, A. van der Zande, J. S. Owen, and T. F. Heinz, Excitons in ultrathin organic-inorganic perovskite crystals, *Phys. Rev. B* 92(4), 045414 (2015)
71. J. Chen, L. Gan, F. Zhuge, H. Li, J. Song, H. Zeng, and T. Zhai, A ternary solvent method for large-sized two-dimensional perovskites, *Angew. Chem. Int. Ed. Engl.* 56(9), 2390 (2017)
72. Y. Liu, Y. Zhang, Z. Yang, H. Ye, J. Feng, Z. Xu, X. Zhang, R. Munir, J. Liu, P. Zuo, Q. Li, M. Hu, L. Meng, K. Wang, D. M. Smilgies, G. Zhao, H. Xu, Z. Yang, A. Amassian, J. Li, K. Zhao, and S. F. Liu, Multi-inch single-crystalline perovskite membrane for high-detectivity flexible photosensors, *Nat. Commun.* 9(1), 5302 (2018)
73. S. T. Ha, X. Liu, Q. Zhang, D. Giovanni, T. C. Sum, and Q. Xiong, Synthesis of organic-inorganic lead halide perovskite nanoplatelets: Towards high-performance perovskite solar cells and optoelectronic devices, *Adv. Opt. Mater.* 2(9), 838 (2014)
74. J. Liu, Y. Xue, Z. Wang, Z. Q. Xu, C. Zheng, B. Weber, J. Song, Y. Wang, Y. Lu, Y. Zhang, and Q. Bao, Two-dimensional $CH_3NH_3PbI_3$ perovskite: Synthesis and optoelectronic application, *ACS Nano* 10(3), 3536 (2016)
75. Y. P. Wang, Y. F. Shi, G. Q. Xin, J. Lan, and J. Shi, Two-dimensional van der waals epitaxy kinetics in a three-dimensional perovskite halide, *Cryst. Growth Des.* 15(10), 4741 (2015)
76. L. Niu, X. Liu, C. Cong, C. Wu, D. Wu, T. R. Chang, H. Wang, Q. Zeng, J. Zhou, X. Wang, W. Fu, P. Yu, Q. Fu, S. Najmaei, Z. Zhang, B. I. Yakobson, B. K. Tay, W. Zhou, H. T. Jeng, H. Lin, T. C. Sum, C. Jin, H. He, T. Yu, and Z. Liu, Controlled synthesis of organic/inorganic van der waals solid for tunable light-matter interactions, *Adv. Mater.* 27(47), 7800 (2015)
77. B. Liu, M. Long, M. Q. Cai, and J. Yang, Two-dimensional van der Waals heterostructures constructed via perovskite $(C_4H_9NH_3)_2XBr_4$ and black phosphorus, *J. Phys. Chem. Lett.* 9(17), 4822 (2018)
78. J. Chen, Y. Wang, L. Gan, Y. He, H. Li, and T. Zhai, Generalized self-doping engineering towards ultrathin and large-sized two-dimensional homologous perovskites, *Angew. Chem. Int. Ed. Engl.* 56(47), 14893 (2017)
79. J. Liu, J. Leng, K. Wu, J. Zhang, and S. Jin, Observation of internal photoinduced electron and hole separation in hybrid two-dimentional perovskite films, *J. Am. Chem. Soc.* 139(4), 1432 (2017)
80. R. Quintero-Bermudez, A. Gold-Parker, A. H. Proppe, R. Munir, Z. Yang, S. O. Kelley, A. Amassian, M. F. Toney, and E. H. Sargent, Compositional and orientational control in metal halide perovskites of reduced dimensionality, *Nat. Mater.* 17(10), 900 (2018)
81. Y. Lin, Y. Fang, J. Zhao, Y. Shao, S. J. Stuard, M. M. Nahid, H. Ade, Q. Wang, J. E. Shield, N. Zhou, A. M. Moran, and J. Huang, Unveiling the operation mechanism of layered perovskite solar cells, *Nat. Commun.* 10(1), 1008 (2019)
82. N. N. Wang, L. Cheng, R. Ge, S. T. Zhang, Y. F. Miao, W. Zou, C. Yi, Y. Sun, Y. Cao, R. Yang, Y. Q. Wei, Q. Guo, Y. Ke, M. T. Yu, Y. Z. Jin, Y. Liu, Q. Q. Ding, D. W. Di, L. Yang, G. C. Xing, H. Tian, C. H. Jin, F. Gao, R. H. Friend, J. P. Wang, and W. Huang, Perovskite light-emitting diodes based on solution-processed self-organized multiple quantum wells, *Nat. Photonics* 10(11), 699 (2016)
83. M. Yuan, L. N. Quan, R. Comin, G. Walters, R. Sabatini, O. Voznyy, S. Hoogland, Y. Zhao, E. M. Beauregard, P. Kanjanaboos, Z. Lu, D. H. Kim, and E. H. Sargent, Perovskite energy funnels for efficient light-emitting diodes, *Nat. Nanotechnol.* 11(10), 872 (2016)
84. J. H. Wang, J. Leng, J. X. Liu, S. He, Y. Wang, K. F. Wu, and S. Y. Jin, Engineered directional charge flow in mixed two-dimensional perovskites enabled by facile cation-exchange, *J. Phys. Chem. C* 121(39), 21281 (2017)
85. Q. Shang, Y. Wang, Y. Zhong, Y. Mi, L. Qin, Y. Zhao, X. Qiu, X. Liu, and Q. Zhang, Unveiling structurally engineered carrier dynamics in hybrid quasi-two-dimensional perovskite thin films toward controllable emission, *J. Phys. Chem. Lett.* 8(18), 4431 (2017)
86. J. Wang, J. Li, Q. Tan, L. Li, J. Zhang, J. Zang, P. Tan, J. Zhang, and D. Li, Controllable synthesis of two-dimensional ruddlesden-popper-type perovskite heterostructures, *J. Phys. Chem. Lett.* 8(24), 6211 (2017)
87. L. Chao, Z. Wang, Y. Xia, Y. Chen, and W. Huang, Recent progress on low dimensional perovskite solar cells, *J. Energy Chem.* 27(4), 1091 (2018)
88. P. Gao, A. R. Bin Mohd Yusoff, and M. K. Nazeeruddin, Dimensionality engineering of hybrid halide perovskite light absorbers, *Nat. Commun.* 9(1), 5028 (2018)
89. G. Grancini, and M. K. Nazeeruddin, Dimensional tailoring of hybrid perovskites for photovoltaics, *Nat. Rev. Mater.* 4(1), 4 (2019)
90. J. L. Yan, W. M. Qiu, G. Wu, P. Heremans, and H. Z. Chen, Recent progress in 2D/quasi-2D layered metal halide perovskites for solar cells, *J. Mater. Chem. A* 6(24), 11063 (2018)

91. S. Li, B. Yang, R. Wu, C. Zhang, C. Zhang, X. F. Tang, G. Liu, P. Liu, C. Zhou, Y. Gao, J. Q. Meng, and J. Yang, High-quality $CH_3NH_3PbI_3$ thin film fabricated via intramolecular exchange for efficient planar heterojunction perovskite solar cells, *Org. Electron.* 39, 304 (2016)

92. T. M. Koh, V. Shanmugam, X. T. Guo, S. S. Lim, O. Filonik, E. M. Herzig, P. Muller-Buschbaum, V. Swamy, S. T. Chien, S. G. Mhaisalkar, and N. Mathews, Enhancing moisture tolerance in efficient hybrid 3D/2D perovskite photovoltaics, *J. Mater. Chem. A* 6(5), 2122 (2018)

93. Y. Cho, A. M. Soufiani, J. S. Yun, J. Kim, D. S. Lee, J. Seidel, X. Deng, M. A. Green, S. Huang, and A. W. Y. Ho-Baillie, Mixed 3D–2D passivation treatment for mixed-cation lead mixed-halide perovskite solar cells for higher efficiency and better stability, *Adv. Energy Mater.* 8(20), 1703392 (2018)

94. C. Ma, C. Leng, Y. Ji, X. Wei, K. Sun, L. Tang, J. Yang, W. Luo, C. Li, Y. Deng, S. Feng, J. Shen, S. Lu, C. Du, and H. Shi, 2D/3D perovskite hybrids as moisture-tolerant and efficient light absorbers for solar cells, *Nanoscale* 8(43), 18309 (2016)

95. Y. Lv, Y. Shi, X. Song, J. Liu, M. Wang, S. Wang, Y. Feng, S. Jin, and C. Hao, Bromine doping as an efficient strategy to reduce the interfacial defects in hybrid two-dimensional/three-dimensional stacking perovskite solar cells, *ACS Appl. Mater. Interfaces* 10(37), 31755 (2018)

96. P. Chen, Y. Bai, S. Wang, M. Lyu, J. H. Yun, and L. Wang, In situ growth of 2D perovskite capping layer for stable and efficient perovskite solar cells, *Adv. Funct. Mater.* 28(17), 1706923 (2018)

97. N. Li, Z. L. Zhu, Q. S. Dong, J. W. Li, Z. L. Yang, C. C. Chueh, A. K. Y. Jen, and L. D. Wang, Enhanced moisture stability of cesium-containing compositional perovskites by a feasible interfacial engineering, *Adv. Mater. Interfaces* 4(20), 1700598 (2017)

98. T. Ye, A. Bruno, G. F. Han, T. M. Koh, J. Li, N. F. Jamaludin, C. Soci, S. G. Mhaisalkar, and W. L. Leong, Efficient and ambient-air-stable solar cell with highly oriented 2D@3D perovskites, *Adv. Funct. Mater.* 28(30), 1801654 (2018)

99. T. Zhao, C. C. Chueh, Q. Chen, A. Rajagopal, and A. K. Y. Jen, Defect passivation of organic–inorganic hybrid perovskites by diammonium iodide toward high-performance photovoltaic devices, *ACS Energy Lett.* 1(4), 757 (2016)

100. Y. Bai, S. Xiao, C. Hu, T. Zhang, X. Meng, H. Lin, Y. Yang, and S. Yang, Dimensional engineering of a graded 3D-2D halide perovskite interface enables ultrahigh V_{oc} enhanced stability in the p-i-n photovoltaics, *Adv. Energy Mater.* 7(20), 1701038 (2017)

101. M. Xiao, F. Huang, W. Huang, Y. Dkhissi, Y. Zhu, J. Etheridge, A. Gray-Weale, U. Bach, Y. B. Cheng, and L. Spiccia, A fast deposition-crystallization procedure for highly efficient lead iodide perovskite thin-film solar cells, *Angew. Chem. Int. Ed. Engl.* 53(37), 9898 (2014)

102. N. J. Jeon, J. H. Noh, Y. C. Kim, W. S. Yang, S. Ryu, and S. I. Seok, Solvent engineering for high-performance inorganic–organic hybrid perovskite solar cells, *Nat. Mater.* 13(9), 897 (2014)

103. B. Liu, M. Long, M. Cai, L. Ding, and J. Yang, Interfacial charge behavior modulation in 2D/3D perovskite heterostructure for potential high-performance solar cells, *Nano Energy* 59, 715 (2019)

104. K. T. Cho, G. Grancini, Y. Lee, E. Oveisi, J. Ryu, O. Almora, M. Tschumi, P. A. Schouwink, G. Seo, S. Heo, J. Park, J. Jang, S. Paek, G. Garcia-Belmonte, and M. K. Nazeeruddin, Selective growth of layered perovskites for stable and efficient photovoltaics, *Energy Environ. Sci.* 11(4), 952 (2018)

105. D. Luo, W. Yang, Z. Wang, A. Sadhanala, Q. Hu, R. Su, R. Shivanna, G. F. Trindade, J. F. Watts, Z. Xu, T. Liu, K. Chen, F. Ye, P. Wu, L. Zhao, J. Wu, Y. Tu, Y. Zhang, X. Yang, W. Zhang, R. H. Friend, Q. Gong, H. J. Snaith, and R. Zhu, Enhanced photovoltage for inverted planar heterojunction perovskite solar cells, *Science* 360(6396), 1442 (2018)

106. Y. Wang, J. Li, Q. Li, W. Zhu, T. Yu, X. Chen, L. Yin, Y. Zhou, X. Wang, and Z. Zou, PbI_2 heterogeneous-cap-induced crystallization for an efficient $CH_3NH_3PbI_3$ layer in perovskite solar cells, *Chem. Commun.* 53(36), 5032 (2017)

107. Q. Chen, H. Zhou, T. B. Song, S. Luo, Z. Hong, H. S. Duan, L. Dou, Y. Liu, and Y. Yang, Controllable self-induced passivation of hybrid lead iodide perovskites toward high performance solar cells, *Nano Lett.* 14(7), 4158 (2014)

108. M. C. Shih, S. S. Li, C. H. Hsieh, Y. C. Wang, H. D. Yang, Y. P. Chiu, C. S. Chang, and C. W. Chen, Spatially resolved imaging on photocarrier generations and band alignments at perovskite/PbI_2 heterointerfaces of perovskite solar cells by light-modulated scanning tunneling microscopy, *Nano Lett.* 17(2), 1154 (2017)

109. T. J. Jacobsson, J. P. Correa-Baena, E. Halvani Anaraki, B. Philippe, S. D. Stranks, M. E. Bouduban, W. Tress, K. Schenk, J. Teuscher, J. E. Moser, H. Rensmo, and A. Hagfeldt, Unreacted PbI_2 as a double-edged sword for enhancing the performance of perovskite solar cells, *J. Am. Chem. Soc.* 138(32), 10331 (2016)

110. S. Chen, X. Wen, J. S. Yun, S. Huang, M. Green, N. J. Jeon, W. S. Yang, J. H. Noh, J. Seo, S. I. Seok, and A. Ho-Baillie, Spatial distribution of lead iodide and local passivation on organo-lead halide perovskite, *ACS Appl. Mater. Interfaces* 9(7), 6072 (2017)

111. F. Liu, Q. Dong, M. K. Wong, A. B. Djurišić, A. Ng, Z. Ren, Q. Shen, C. Surya, W. K. Chan, J. Wang, A. M. C. Ng, C. Liao, H. Li, K. Shih, C. Wei, H. Su, and J. Dai, Is excess PbI_2 beneficial for perovskite solar cell performance? *Adv. Energy Mater.* 6(7), 1502206 (2016)

112. Y. Lin, Y. Bai, Y. Fang, Z. Chen, S. Yang, X. Zheng, S. Tang, Y. Liu, J. Zhao, and J. Huang, Enhanced thermal stability in perovskite solar cells by assembling 2D/3D stacking structures, *J. Phys. Chem. Lett.* 9(3), 654 (2018)

113. F. Wang, W. Geng, Y. Zhou, H. H. Fang, C. J. Tong, M. A. Loi, L. M. Liu, and N. Zhao, Phenylalkylamine passivation of organolead halide perovskites enabling high-efficiency and air-stable photovoltaic cells, *Adv. Mater.* 28(45), 9986 (2016)

114. J. W. Lee, Z. Dai, T. H. Han, C. Choi, S. Y. Chang, S. J. Lee, N. De Marco, H. Zhao, P. Sun, Y. Huang, and Y. Yang, 2D perovskite stabilized phase-pure formamidinium perovskite solar cells, *Nat. Commun.* 9(1), 3021 (2018)

115. K. T. Cho, Y. Zhang, S. Orlandi, M. Cavazzini, I. Zimmermann, A. Lesch, N. Tabet, G. Pozzi, G. Grancini, and M. K. Nazeeruddin, Water-repellent low-dimensional fluorous perovskite as interfacial coating for 20% efficient solar cells, *Nano Lett.* 18(9), 5467 (2018)

116. G. Jia, Z. J. Shi, Y. D. Xia, Q. Wei, Y. H. Chen, G. C. Xing, and W. Huang, Super air stable quasi-2D organic-inorganic hybrid perovskites for visible light-emitting diodes, *Opt. Express* 26(2), A66 (2018)

117. J. Schlipf, Y. H. Hu, S. Pratap, L. Biessmann, N. Hohn, L. Porcar, T. Bein, P. Docampo, and P. Muller-Buschbaum, Shedding light on the moisture stability of 3D/2D hybrid perovskite heterojunction thin films, *ACS Appl. Energy Mater.* 2(2), 1011 (2019)

118. T. M. Koh, K. Thirumal, H. S. Soo, and N. Mathews, Multidimensional perovskites: A mixed cation approach towards ambient stable and tunable perovskite photovoltaics, *ChemSusChem* 9(18), 2541 (2016)

119. Z. Xiao, Y. Yuan, Y. Shao, Q. Wang, Q. Dong, C. Bi, P. Sharma, A. Gruverman, and J. Huang, Giant switchable photovoltaic effect in organometal trihalide perovskite devices, *Nat. Mater.* 14(2), 193 (2015)

120. Y. Yuan and J. Huang, Ion migration in organometal trihalide perovskite and its impact on photovoltaic efficiency and stability, *Acc. Chem. Res.* 49(2), 286 (2016)

121. Y. Yuan, T. Li, Q. Wang, J. Xing, A. Gruverman, and J. Huang, Anomalous photovoltaic effect in organic-inorganic hybrid perovskite solar cells, *Sci. Adv.* 3(3), e1602164 (2017)

122. Y. Lin, Y. Bai, Y. J. Fang, Q. Wang, Y. H. Deng, and J. S. Huang, Suppressed ion migration in low-dimensional perovskites, *ACS Energy Lett.* 2(7), 1571 (2017)

123. X. Xiao, J. Dai, Y. J. Fang, J. J. Zhao, X. P. Zheng, S. Tang, P. N. Rudd, X. C. Zeng, and J. S. Huang, Suppressed ion migration along the in-plane direction in layered perovskites, *ACS Energy Lett.* 3(3), 684 (2018)

124. Z. Li, M. J. Yang, J. S. Park, S. H. Wei, J. J. Berry, and K. Zhu, Stabilizing perovskite structures by tuning tolerance factor: Formation of formamidinium and cesium lead iodide solid-state alloys, *Chem. Mater.* 28(1), 284 (2016)

125. T. Zhang, M. I. Dar, G. Li, F. Xu, N. Guo, M. Gratzel, and Y. Zhao, Bication lead iodide 2D perovskite component to stabilize inorganic alpha-CsPbI3 perovskite phase for high-efficiency solar cells, *Sci. Adv.* 3(9), e1700841 (2017)

126. E. Yassitepe, Z. Y. Yang, O. Voznyy, Y. Kim, G. Walters, J. A. Castaeda, P. Kanjanaboos, M. J. Yuan, X. W. Gong, F. J. Fan, J. Pan, S. Hoogland, R. Comin, O. M. Bakr, L. A. Padilha, A. F. Nogueira, and E. H. Sargent, Amine-free synthesis of cesium lead halide perovskite quantum dots for efficient light-emitting diodes, *Adv. Funct. Mater.* 26(47), 8757 (2016)

127. J. Li, L. Xu, T. Wang, J. Song, J. Chen, J. Xue, Y. Dong, B. Cai, Q. Shan, B. Han, and H. Zeng, 50-fold EQE improvement up to 6.27% of solution-processed all-inorganic perovskite $CsPbBr_3$ QLEDs via surface ligand density control, *Adv. Mater.* 29(5), 1603885 (2017)

128. C. Sun, Y. Zhang, C. Ruan, C. Yin, X. Wang, Y. Wang, and W. W. Yu, Efficient and stable white LEDs with silica-coated inorganic perovskite quantum dots, *Adv. Mater.* 28(45), 10088 (2016)

129. A. Swarnkar, A. R. Marshall, E. M. Sanehira, B. D. Chernomordik, D. T. Moore, J. A. Christians, T. Chakrabarti, and J. M. Luther, Quantum dot-induced phase stabilization of alpha-$CsPbI_3$ perovskite for high-efficiency photovoltaics, *Science* 354(6308), 92 (2016)

130. E. M. Sanehira, A. R. Marshall, J. A. Christians, S. P. Harvey, P. N. Ciesielski, L. M. Wheeler, P. Schulz, L. Y. Lin, M. C. Beard, and J. M. Luther, Enhanced mobility $CsPbI_3$ quantum dot arrays for record-efficiency, high-voltage photovoltaic cells, *Sci. Adv.* 3(10), eaao4204 (2017)

131. P. F. Li, B. N. Shivananju, Y. P. Zhang, S. J. Li, and Q. L. Bao, High performance photodetector based on 2D $CH_3NH_3PbI_3$ perovskite nanosheets, *J. Phys. D Appl. Phys.* 50(9), 094002 (2017)

132. Z. Tan, Y. Wu, H. Hong, J. Yin, J. Zhang, L. Lin, M. Wang, X. Sun, L. Sun, Y. Huang, K. Liu, Z. Liu, and H. Peng, Two-dimensional $(C_4H_9NH_3)_2PbBr_4$ perovskite crystals for high-performance photodetector, *J. Am. Chem. Soc.* 138(51), 16612 (2016)

133. Q. Zhang, S. T. Ha, X. Liu, T. C. Sum, and Q. Xiong, Room-temperature near-infrared high-Q perovskite whispering-gallery planar nanolasers, *Nano Lett.* 14(10), 5995 (2014)

134. H. Zhu, Y. Fu, F. Meng, X. Wu, Z. Gong, Q. Ding, M. V. Gustafsson, M. T. Trinh, S. Jin, and X. Y. Zhu, Lead halide perovskite nanowire lasers with low lasing thresholds and high quality factors, *Nat. Mater.* 14(6), 636 (2015)

135. P. Tyagi, S. M. Arveson, and W. A. Tisdale, Colloidal organohalide perovskite nanoplatelets exhibiting quantum confinement, *J. Phys. Chem. Lett.* 6(10), 1911 (2015)

136. Y. Bekenstein, B. A. Koscher, S. W. Eaton, P. Yang, and A. P. Alivisatos, Highly luminescent colloidal nanoplates of perovskite cesium lead halide and their oriented assemblies, *J. Am. Chem. Soc.* 137(51), 16008 (2015)

137. O. Vybornyi, S. Yakunin, and M. V. Kovalenko, Polar-solvent-free colloidal synthesis of highly luminescent alkylammonium lead halide perovskite nanocrystals, *Nanoscale* 8(12), 6278 (2016)

138. H. Huang, L. Polavarapu, J. A. Sichert, A. S. Susha, A. S. Urban, and A. L. Rogach, Colloidal lead halide perovskite nanocrystals: Synthesis, optical properties and applications, *NPG Asia Mater.* 8(11), e328 (2016)

139. F. Zhang, H. Zhong, C. Chen, X. G. Wu, X. Hu, H. Huang, J. Han, B. Zou, and Y. Dong, Brightly luminescent and color-tunable colloidal $CH_3NH_3PbX_3$ (X = Br, I, Cl) quantum dots: Potential alternatives for display technology, *ACS Nano* 9(4), 4533 (2015)

140. F. Zhu, L. Men, Y. Guo, Q. Zhu, U. Bhattacharjee, P. M. Goodwin, J. W. Petrich, E. A. Smith, and J. Vela, Shape evolution and single particle luminescence of organometal halide perovskite nanocrystals, *ACS Nano* 9(3), 2948 (2015)

141. Z. Liang, S. Zhao, Z. Xu, B. Qiao, P. Song, D. Gao, and X. Xu, Shape-controlled synthesis of all-inorganic $CsPbBr_3$ perovskite nanocrystals with bright blue emission, *ACS Appl. Mater. Interfaces* 8(42), 28824 (2016)

142. J. A. Sichert, Y. Tong, N. Mutz, M. Vollmer, S. Fischer, K. Z. Milowska, R. Garcia Cortadella, B. Nickel, C. Cardenas-Daw, J. K. Stolarczyk, A. S. Urban, and J. Feldmann, Quantum size effect in organometal halide perovskite nanoplatelets, *Nano Lett.* 15(10), 6521 (2015)

143. S. Sun, D. Yuan, Y. Xu, A. Wang, and Z. Deng, Ligand-mediated synthesis of shape-controlled cesium lead halide perovskite nanocrystals via reprecipitation process at room temperature, *ACS Nano* 10(3), 3648 (2016)

144. V. A. Hintermayr, A. F. Richter, F. Ehrat, M. Doblinger, W. Vanderlinden, J. A. Sichert, Y. Tong, L. Polavarapu, J. Feldmann, and A. S. Urban, Tuning the optical properties of perovskite nanoplatelets through composition and thickness by ligand-assisted exfoliation, *Adv. Mater.* 28(43), 9478 (2016)

145. Y. Tong, F. Ehrat, W. Vanderlinden, C. Cardenas-Daw, J. K. Stolarczyk, L. Polavarapu, and A. S. Urban, Dilution-induced formation of hybrid perovskite nanoplatelets, *ACS Nano* 10(12), 10936 (2016)